NASA Technical Memorandum 104245

Piloted Simulation Study of a Balloon-Assisted Deployment of an Aircraft at High Altitude

James Murray, Timothy Moes, Ken Norlin, Jeffrey Bauer,
Robert Geenen, Bryan Moulton, and Stephen Hoang

January 1992

National Aeronautics and
Space Administration

NASA Technical Memorandum 104245

Piloted Simulation Study of a Balloon-Assisted Deployment of an Aircraft at High Altitude

James Murray, Timothy Moes, Ken Norlin, and Jeffrey Bauer
NASA Dryden Flight Research Facility, Edwards, California

Robert Geenen and Bryan Moulton
PRC Inc., Edwards, California

Stephen Hoang
NASA Dryden Flight Research Facility, Edwards, California

1992

NASA
National Aeronautics and
Space Administration
Dryden Flight Research Facility
Edwards, California 93523-0273

CONTENTS

ABSTRACT

A real-time piloted simulation at the NASA Dryden Flight Research Facility (NASA Dryden) was used to study the feasibility of a balloon-assisted deployment of a research aircraft at high altitude. In the simulation study, an unmanned, modified sailplane was carried to 110,000 ft with a high-altitude balloon and released in a nosedown attitude. A remote pilot controlled the aircraft through a near-maximum-lift pullout and then executed a zoom climb to a trimmed, 1-g flight condition. A small parachute was used to limit the Mach number during the pullout to avoid adverse transonic effects and their resultant energy losses. The use of a small rocket motor was investigated for increasing the maximum attainable altitude.

Aerodynamic modifications to the basic sailplane included applying supercritical airfoil gloves over the existing wing and tail surfaces. The performance of the simulated aircraft was based on low Reynolds number wind-tunnel tests and computational techniques. The aerodynamic model included significant Mach number and Reynolds number effects at high altitude.

Parametric variations were performed to study the effects of launch altitude, gross weight, Mach number limit, and parachute size on the maximum attainable stabilized altitude. A test altitude of approximately 95,000 ft was attained, and altitudes in excess of 100,000 ft were attained with small amounts of rocket motor assist. A discussion of the utility of this deployment technique for atmospheric science mission and other high-altitude aircraft is included.

INTRODUCTION

Recent world events have thrust environmental issues to the forefront of national and international consciousness. Widespread attention has focused on the changes in global atmospheric chemistry and the potential effects on planetary climate and habitability. Global atmospheric change (the proliferation of greenhouse gases in the troposphere and the depletion of ozone in the stratosphere) is significant and measurable (Ember et al., 1986). The atmospheric science community has mobilized to gain an understanding of the physical, chemical, and biological processes at work. Validation of the candidate dynamic models and testing of the proposed hypotheses require vast amounts of scientific data from the upper atmosphere. The approach to data acquisition is multifaceted. Ground-based and space-based platforms make remote measurements, while high-altitude balloons, rockets, and manned and unmanned aircraft make direct *in-situ* measurements; however, additional capability is required. At a recent workshop (*Global Stratospheric Change,* 1989), the science community defined requirements for an Antarctic atmospheric sampling mission platform with altitude and range performance greatly exceeding that of currently available aircraft. Workshop specifications call for a transonic aircraft capable of long-range cruise (5000 nmi) at high altitude (100,000 ft), with popup capability to extreme altitude (130,000 ft).

Development of a powered aircraft to fly at transonic speeds at altitudes (H) near 100,000 ft presents a formidable engineering challenge (Sim, 1991, and Russell et al., 1991). Nevertheless, proposed and actual flight vehicles are approaching this altitude. As early as 1978, prototypes of the Mini-Sniffer high-altitude remotely piloted vehicle (RPV) (Reed, 1978) were flight-tested at low altitude. The ER-2 and the Condor aircraft (Boeing Company, Seattle, Washington) (Henderson, 1990) have 60,000 to 70,000 ft altitude capability, and the Perseus aircraft (Aurora Flight Sciences, Manassas, Virginia) (Russell et al., 1991) currently in flight test is designed to reach 82,000-ft altitude. A number of aircraft concepts (Sim, 1991, Chambers, 1990, Russell et al., 1991, and DeLaurier et al., 1986) study flight at 100,000-ft altitude. These conceptual studies are limited by the lack of aerodynamic data for low Reynolds number, transonic flight conditions.

Aircraft with practical wing loadings flying at altitudes near 100,000 ft will, by necessity, operate at transonic speeds and at Reynolds numbers well below one million. A generalized altitude/Mach number (M) flight envelope for such aircraft is shown in figure 1 with trajectories of constant dynamic pressure ($\bar{q}$) and constant Reynolds number (Rn) per unit foot superimposed. For this flight regime, computational (Drela, 1987) and wind-tunnel

techniques are currently the only design and development tools available; neither has been validated with flight data. Although wind tunnels have been used for collecting extensive data at low Reynolds number and low speed (Carmichael, 1981 and Mueller, 1985), wind-tunnel data at low Reynolds number and transonic speeds are very limited.

An Apex aircraft is proposed as an aerodynamic research test bed that would efficiently collect low-turbulence, low Reynolds number, transonic flight data for validation and calibration of wind-tunnel and computational techniques. This would in turn lead to the development of effective high-altitude aircraft for atmospheric research and other applications.

Timely acquisition of baseline aerodynamic flight data is critical to ongoing design and development efforts for high-altitude aircraft. Deploying an aerodynamic research aircraft such as the Apex aircraft with a high-altitude balloon has great potential for acquiring baseline aerodynamic flight data very quickly. By using the proven balloon-deployment capability of the National Scientific Balloon Facility (Peterson, 1991) and eliminating the time associated with the development of a high-altitude power-plant, a balloon-deployed research aircraft can potentially acquire the necessary aerodynamic flight data sooner and more cost-effectively than a conventionally-powered, runway-deployed vehicle.

A simulation study was conducted to address the technical issues of the proposed high-altitude balloon-deployment technique. This paper investigates one critical technical issue: the viability of launching the aircraft from a balloon at high altitude and successfully flying a pullout maneuver to a trimmed, 1-g flight condition of at least 100,000-ft altitude. The investigation had three objectives. The primary objective was to determine if the balloon launch and pullout could be executed successfully while remaining within the allowed flight envelope of the Apex aircraft. Once this objective was met, the secondary objective was to characterize the sensitivity of the final, trimmed altitude (H_f) to variations in simulation parameters. The final objective was to develop techniques for using a small rocket motor to increase H_f to at least 100,000 ft.

NOMENCLATURE

Symbols

AR	aspect ratio
a_n	normal acceleration, or load factor, g
b	reference span, ft
c	reference chord, ft
c.g.	center of gravity
E	total energy (*potential* + *kinetic*), referenced to condition of zero velocity at the balloon release altitude, ft·lb
H	pressure altitude, ft
I_{XX}	rolling moment of inertia, slug-ft^2
I_{XZ}	X–Z cross product of inertia, slug-ft^2
I_{YY}	pitching moment of inertia, slug-ft^2
I_{ZZ}	yawing moment of inertia, slug-ft^2
M	Mach number
mg	aircraft gross weight, lb
q	pitch rate, deg/sec

$\bar{q}$	dynamic pressure, lb/ft^2
R	parachute radius, ft
Rn	Reynolds number
S	reference area, ft^2
t	time from balloon release, sec
V	true airspeed, ft/sec
X	horizontal distance from balloon release, ft

Greek Symbols

α	angle of attack, deg
γ	flightpath angle, deg
δ_e	elevator deflection, deg
ϵ	span efficiency
θ	body-axis pitch angle, deg

Aerodynamic Coefficients

C_D	vehicle drag coefficient
C_L	vehicle lift coefficient
C_m	pitching moment coefficient

Aerodynamic Derivatives

C_{D_α}	partial derivative of C_D with respect to α, per deg
$C_{D_{\delta_e}}$	partial derivative of C_D with respect to δ_e, per deg
C_{L_q}	partial derivative of C_L with respect to $\frac{qc}{2V}$, per rad
C_{L_α}	partial derivative of C_L with respect to α, per deg
$C_{L_{\delta_e}}$	partial derivative of C_L with respect to δ_e, per deg
C_{m_q}	partial derivative of C_m with respect to $\frac{qc}{2V}$, per rad
C_{m_α}	partial derivative of C_m with respect to α, per deg
$C_{m_{\delta_e}}$	partial derivative of C_m with respect to δ_e, per deg

Subscripts

basic	value of aerodynamic coefficient at $\delta_e = 0°$ and $q = 0$ deg/sec
chute	value for parachute
$C_{L_{max}}$	value at maximum lift coefficient
f	final condition of launch, when stabilized at 1-g flight

i	initial condition of launch
lim	limit value used in simulation study
max	maximum value
wave	due to transonic effects
0	value of aerodynamic coefficient at $\alpha = 0°$, $\delta_e = 0°$, and $q = 0$ deg/sec

Acronyms

LinAir	panel method code
NASA	National Aeronautics and Space Administration
PANDA	Program for Analysis and Design of Airfoils
RPV	remotely piloted vehicle

AIRCRAFT DESCRIPTION AND FLIGHT PROFILE

The Apex aircraft is based on modifications to a Schweizer SGS 1-36 sailplane. The Apex aircraft retains the basic structure of the Schweizer sailplane; significant aerodynamic modifications allow the Apex aircraft to fly at higher Mach numbers. Supercritical airfoil gloves are applied over the existing wing and tail surfaces; the wing and horizontal tail chords are increased by 16.5 percent. The control surface actuation system of the Schweizer sailplane is modified to allow remote control of the Apex aircraft. Figure 2 is a three-view drawing showing the basic Schweizer sailplane and the external modifications needed to make the Apex research aircraft.

Figure 3 shows a schematic of a proposed research flight of the Apex aircraft. The aircraft is carried to 110,000 ft with a high-altitude balloon for release in a nosedown attitude. The pilot controls the aircraft remotely through a near-maximum-lift pullout and then executes a zoom climb to a trimmed, 1-g flight condition. At the high-altitude test condition, the pilot flies a number of research maneuvers; flight control information and research data are telemetered to the ground. At the conclusion of the flight, the pilot lands the aircraft horizontally.

Several operational and performance constraints limit the allowed maneuvering envelope of the aircraft. Figure 4 shows the basic flight envelope of the Apex aircraft in altitude/Mach number form. Included is that portion of the envelope corresponding to the transition from balloon release to trimmed, 1-g flight. The Mach number limit is 0.75; beyond this value adverse transonic effects cause rapid performance degradation and the potential for structural failure. The stall limit corresponds to an angle of attack (α) of approximately 6° at 100,000-ft altitude; this is the angle-of-attack limit during the pullout. For the altitudes of the launch study, there is effectively no dynamic pressure limit; for altitudes greater than 75,000 ft the Mach number limit supersedes the dynamic pressure limit. The load factor limit for the modified sailplane is 2.5 g.

SIMULATION AND AIRCRAFT MODELING

Simulation–Simulator Description Overview

The Apex simulation uses nonlinear, rigid-body, six-degree-of-freedom equations of motion (Maine, 1986). The simulation is hosted on a Gould 32/9780 computer (Encore Computer Corp., Fort Lauderdale, Florida) and is programmed in FORTRAN 77 with some machine-specific assembly language routines. There is a real-time pilot-in-the-loop and a nonreal-time or batch version of the Apex simulation. The real-time simulation operates at

100 frames/sec. The atmospheric model was derived from the *U. S. Standard Atmosphere, 1962* and was implemented as a table look up scheduled with altitude. The aerodynamic model described as follows was implemented in the simulation as a set of table look ups scheduled with angle of attack, Mach number, and pressure altitude. The simulation uses a modified second-order Runge-Kutta integration algorithm for computing state variables. Actuator dynamics were not modeled and no control system was used for this study.

The simulator hardware used in this study is a fixed-base cockpit with a full array of cockpit instruments and a computer-generated, out-the-windscreen graphics display with an overlaid head-up display. Pilot controls include an electronic stick and rudder pedals with centering forces; trim switches are included for zeroing the centering forces at trim conditions. Additional simulator controls include an array of switches for implementing auxiliary controls and changing simulation modes. Figure 5 is a photograph of the simulator cockpit.

Two special features not normally found on simulators at NASA Dryden were added to the Apex simulation for this study. Some launch techniques used a small parachute; a simple parachute model was added to the simulation. There are no dynamics associated with the chute deployment or the attachment of the chute to the aircraft. The chute, when deployed, simply provides a force and moment increment based on the selected chute size, drag coeffiecient, and attachment point. The pilot controls the chute deployment and release through a simulator cockpit switch. The mass of the parachute is not currently included in the simulation.

Some launch techniques used a small rocket motor; a simple rocket model was added to the simulation. The force and moment increment generated by the rocket motor is based on the selected thrust, attachment point, and attachment orientation in the aircraft model. The pilot controls the ignition and shutdown of the rocket motor through a cockpit simulator switch. The mass of the rocket motor is not currently included in the simulation.

Aerodynamic Model

The aerodynamic model for the Apex airplane was based on modifications to a Schweizer SGS 1-36 sailplane. The aerodynamic modifications include applying gloved airfoil sections over the existing wing, horizontal tail, and vertical tail. The OW 70-10-14mod airfoil (Kennelly et al., 1990) used to glove the wing is shown compared with the original Schweizer FX61-163 airfoil in figure 6. This supercritical airfoil designed for the NASA F-8 Oblique Wing Program was chosen for this study for two reasons: it has a design Mach number of 0.70 and some low Reynolds number, transonic wind-tunnel data (still unpublished) exist for this airfoil.

The Apex aerodynamic model was developed using a combination of computational techniques, wind-tunnel test results for the OW 70-10-14mod airfoil, flight test results, and handbook methods. The panel method code (LinAir) (*LinAir for the Macintosh, Version 3.3–LinAir Pro.*, 1987) was used in the computation of some of the longitudinal aerodynamic derivatives. The LinAir program solves the Prandtl-Glauert equation for inviscid, irrotational, and subsonic flow. The wing and horizontal tail surfaces of the Apex aircraft were paneled as shown in figure 7 for analysis with LinAir. The Program for Analysis and Design of Airfoils (PANDA) (*PANDA–A Program for Analysis and Design of Airfoils*, 1988), a two-dimensional airfoil code, was also used in the computation of some aerodynamic derivatives. The PANDA program uses a superposition of sources and vortexes to compute the inviscid pressure distribution, and therefore airfoil lift and drag.

Flight data for a basic Schweizer sailplane were obtained during a flight research program previously conducted at NASA Dryden using a Schweizer SGS 1-36 sailplane. A complete set of stability and control derivatives was obtained over a large flight envelope (Sim, 1990). Some of these test results were used in the development of the Apex aerodynamic model.

Although a large-envelope, six-degree-of-freedom simulation was used, only the low-angle-of-attack longitudinal model is relevant to this study and is discussed in detail. The simulation uses the following equations for the longitudinal aerodynamic model lift coefficient (C_L), drag coefficient (C_D), and pitching moment coefficient (C_m):

$$C_L = C_{L_{basic}}(\alpha) + C_{L_q}\frac{qc}{2V} + C_{L_{\delta_e}}\delta_e$$
$$C_D = C_{D_{basic}}(\alpha) + C_{D_{\delta_e}}\delta_e$$
$$C_m = C_{m_{basic}}(\alpha) + C_{m_q}\frac{qc}{2V} + C_{m_{\delta_e}}\delta_e$$

The model for lift coefficient ($C_{L_{basic}}$) was developed using a variety of techniques and data sources. Maximum lift coefficient occurs at an angle of attack of $\alpha_{C_{L_{max}}}$. For angles of attack below $\alpha_{C_{L_{max}}}$, $C_{L_{basic}}$ was modeled as a linear function of angle of attack:

$$C_{L_{basic}}(\alpha) = C_{L_0} + C_{L_\alpha}\alpha$$

The PANDA program was used to compute C_{L_0} as a function of Mach number, and LinAir was used to compute C_{L_α} as a function of Mach number. Values of $C_{L_{max}}$ were estimated from wind-tunnel data as functions of both Mach number and Reynolds number. The values of C_{L_0}, C_{L_α}, and $C_{L_{max}}$ completely defined $C_{L_{basic}}$ for angles of attack up to $\alpha_{C_{L_{max}}}$.

At Mach numbers of approximately 0.75 and greater, shock formation on the OW 70-10-14mod airfoil severely degrades $C_{L_{basic}}$. These transonic effects were modeled using wind-tunnel data and trends shown in an aerodynamic handbook (Roskam, 1979) for a thick, unswept, high-aspect-ratio wing.

Combining all of the previous data, $C_{L_{basic}}$ for the complete flight envelope of the Apex aircraft is defined. Figure 8 shows $C_{L_{basic}}$ as a function of angle of attack and Mach number for the altitudes used in the aerodynamic model. The values of C_{L_q} and $C_{L_{\delta_e}}$ were taken directly from the flight test results of Sim, 1990.

Drag coefficient ($C_{D_{basic}}$) is modeled with the following equation:

$$C_{D_{basic}}(\alpha) = C_{D_0} + \frac{C_{L^2}(\alpha)}{\pi AR\epsilon} + \Delta C_{D_{wave}}$$

where

$$C_{D_0} = 0.02$$
$$AR = 13$$
$$\epsilon = 0.75$$

The value of C_{D_0} selected is representative of this class of aircraft. Aspect ratio (AR) is that of the Apex configuration, and the value of span efficiency (ϵ) was computed using LinAir. The transonic wave drag term, ($\Delta C_{D_{wave}}$) is an empirical estimate based on extrapolation of aerodynamic handbook values (Jones, 1960) to an airfoil of 14-percent thickness.

The equation for $C_{D_{basic}}$ was used for angles of attack up to $\alpha_{C_{L_{max}}}$. Figure 9 shows $C_{D_{basic}}$ as a function of angle of attack and Mach number for the altitudes used in the aerodynamic model. The values of $C_{D_{\delta_e}}$ were taken directly from the flight test results of Sim, 1990.

The pitching moment coefficient ($C_{m_{basic}}$) was derived using flight test results of Sim, 1990 as an initial estimate. An increment to these values was computed using the LinAir code. For the Sim, 1990 and the Apex configurations, the LinAir code was used to compute values of $C_{m_{basic}}$ as a function of angle of attack and Mach number. The difference between the values for the Apex aircraft and the Sim, 1990 configurations was added to the flight test results. The values of $C_{m_{\delta_e}}$ and C_{m_q} were taken directly from the flight test results of Sim, 1990.

The drag coefficient of the parachute was fixed at 1.0 and was based on the reference area of the parachute, $S_{chute} = \pi R^2$.

Mass Model

The mass model for the Apex aircraft was derived using the Schweizer sailplane as a baseline. The mass of all hardware associated with controlling the aircraft from the cockpit was removed. The mass of the RPV control system and actuators, instrumentation and telemetry systems, video downlink, radar beacon, batteries, wing and tail airfoil gloves, and emergency recovery system were added. The locations of the added masses were adjusted to keep the center of gravity (c.g.) at the same location as that of the Schweizer sailplane. Table 1 shows the physical and mass properties of the Apex aircraft and the basic Schweizer sailplane.

SIMULATED LAUNCH STUDIES

Unassisted Launch

Figure 10 shows the time history of a simulated balloon launch from 110,000-ft altitude without assistance from a parachute or a rocket. Figure 11 shows the aircraft trajectory; 10-sec time intervals are marked on the trajectory to allow comparison with the corresponding time history plots. The Apex aircraft is initially suspended beneath the balloon in a nosedown attitude at zero airspeed. Initial conditions are altitude (H_i) = 110,000 ft, angle of attack (α_i) = 1°, pitch angle (θ_i) = −89°, and airspeed (V_i) = 0 ft/sec. The pilot releases the Apex aircraft from the balloon at time (t) = 0 sec; the Apex aircraft accelerates straight down at 1 g. Pilot control motions, represented by elevator deflection (δ_e), have very little effect until approximately t = 3 sec. That is when the dynamic pressure, $\bar{q}$, is high enough for the pilot's elevator inputs to control the pitch attitude of the Apex aircraft. The pilot controls elevator deflection to hold angle of attack at a near-maximum-lift condition of approximately 6°, and attempts to hold it at that level throughout the pullout. The dynamic pressure is still too low to generate enough lift to significantly affect the flightpath angle (γ); angle of attack has increased, but the velocity vector is still pointing straight down. It is not until t = 15 sec that the velocity vector has been rotated to 10° past the vertical axis (γ = −80°). As the Apex aircraft continues to accelerate, the rapidly increasing lift begins curving the flightpath angle toward the horizontal axis.

At t = 24 sec, as the Apex aircraft accelerates through Mach 0.75, shock-induced losses begin to seriously degrade performance. As discussed earlier, at Mach numbers greater than 0.75, C_L shows a dramatic decrease (fig. 8) and C_D shows a dramatic increase (fig. 9). Even as dynamic pressure continues to increase, C_L falls off so rapidly that the resulting lift is essentially constant for several seconds. Mach number peaks at 0.91 and C_L drops to 0.4 at t = 37 sec. The Apex aircraft begins decelerating and dynamic pressure continues to rise as the Apex aircraft descends in the atmosphere. At t = 50 sec, dynamic pressure peaks at 23 lb/ft^2, and the flightpath angle is approaching the horizontal axis. The pilot begins to decrease angle of attack in anticipation of the upcoming zoom climb. The pilot continues to decrease angle of attack as the Apex aircraft reaches a minimum altitude of 86,500 ft at t = 56 sec, and a maximum normal acceleration (a_n) of 2.5 g at t = 59 sec. The pilot unloads the aircraft slightly for the zoom climb, trading excess speed for altitude to reach a trimmed 1-g flight condition with a final Mach number (M_f) of 0.50 and a final altitude (H_f) of 92,800 ft at t = 95 sec.

This unassisted launch of the Apex aircraft from an altitude of 110,000 ft violates the Mach number limit of the aircraft flight envelope, and therefore does not satisfy the objectives of the simulation study. Even if the Apex flight envelope were expanded to include the flight conditions of the unassisted launch, this launch technique is inefficient from an energy-conservation standpoint. The wave drag at elevated Mach numbers dissipates much of the available potential energy; figure 10 shows that the energy lost between t = 30 and 50 sec is particularly extreme.

Parachute-Assisted Launch

In the following study, a small parachute was used to keep the maximum Mach number (M_{max}) during the pullout within the flight envelope of the Apex aircraft. The parachute was modeled as fully deployed at the launch of the

aircraft from the balloon. The parachute radius (R) of 4.2 ft was determined experimentally to keep the maximum Mach number below a previously-set limit of 0.70. The release point for the chute was determined experimentally such that the maximum Mach number after chute release did not exceed the maximum Mach number reached before chute release.

Figure 12 shows the time history of a simulated parachute-assisted balloon launch from 110,000-ft altitude. Figure 13 shows the aircraft trajectory; 10-sec time intervals are marked on the trajectory to allow comparison with the corresponding time history plots. Launch and the first 5 sec of the parachute-assisted launch are virtually identical to those of the unassisted launch; minor differences are attributable to differences in piloting technique. From t = 15 to 40 sec, the parachute drag is significant, limiting the Mach number rise and allowing the Apex aircraft to maintain a high lift coefficient, C_L. The Mach number peaks at 0.70 at t = 33 sec and the Apex aircraft begins decelerating; $\bar{q}$ continues to rise and peaks at t = 38 sec at 9.5 lb/ft^2. The pilot releases the parachute at t = 40 sec while the flightpath angle is still below the horizontal axis, and the Apex aircraft begins accelerating. Mach number reaches 0.70 again and a_n peaks at 2.1 g at t = 46 sec. The pilot begins decreasing angle of attack for the upcoming zoom climb. The Apex aircraft passes through a minimum altitude of 92,500 ft at t = 49 sec, and the pilot unloads the aircraft to perform a zoom climb to a stabilized flight condition of M_f = 0.50 and H_f = 95,100 ft at t = 80 sec. The use of a small parachute increases H_f by approximately 2300 ft.

Parametric Variations and the Effects on Final Altitude

By providing enough drag to keep the Apex aircraft within the allowable Mach number limit of the flight envelope, the parachute-assisted launch technique satisfied the primary objective of the simulation study. Next the simulation was used to address the second study objective: to investigate the sensitivity of H_f to variations in simulation parameters. The piloted simulation was a very useful tool for efficiently performing such a parametric variation study. The study encompassed the effects of variations in the values of four simulation parameters: initial launch altitude (H_i), aircraft gross weight (mg), parachute radius (R), and Mach number limit (M_{lim}).

The Mach number limit parameter, M_{lim}, was a key concept used throughout the parametric variation study that requires some explanation. This was not an explicit simulation input parameter, but an artificial constraint placed on the flight envelope for the purposes of the study alone. For a given simulation test case, the aircraft was not allowed to exceed M_{lim}. If it did, then the parachute radius was increased as required to maintain Mach number below the predetermined M_{lim}, and the test case was rerun. The correct parachute radius was determined by an iterative technique.

The four parameters are strongly interrelated. For example, for fixed gross weight and M_{lim}, the required parachute radius increases with increasing H_i. Likewise, for fixed H_i and M_{lim}, larger gross weights require larger parachutes. Figure 14 shows this relationship for H_i = 110,000 ft and M_{lim} = 0.70. Finally, for fixed H_i and gross weight, larger M_{lim} values allow smaller chutes to be used. Figure 15 shows this relationship for H_i = 110,000 ft and mg = 869 lb. The results of this parameter sensitivity study are not explicitly shown as a function of parachute radius; however, variations in parachute radius are implicit in most of the results.

There is an upper limit on the final altitude attainable based on conversion of potential energy to kinetic energy. For example, perfect conversion of the potential energy from a balloon release at H_i = 110,000 ft yields a final condition of H_f = 104,400 ft at M_f = 0.60.

Figure 16 shows the variation in H_f, as a function of M_{lim}, for several values of mg. Initial altitude, H_i = 110,000 ft, and the altitude corresponding to perfect conversion of potential energy to a flight condition of Mach 0.60 at 104,400-ft altitude, are also shown on the figure for comparison. For the hypothetical perfect energy conversion case, H_f is independent of gross weight. For the realistic system with energy dissipation modeled, the effect of increasing gross weight on H_f is intuitive; an increase in mg yields a significant decrease in H_f. The effect is directly attributable to the dissipation of energy in drag. As gross weight increases *with fixed* $C_{L_{max}}$, the maximum attainable load factor decreases and the radius of curvature of the flightpath increases. A heavier aircraft

turns toward the horizontal axis more slowly, and accelerates more quickly. A larger parachute is required to limit Mach number buildup, and the larger parachute dissipates more energy in drag.

As shown in figure 16, the reason for the variation in H_f, as a function of M_{lim}, is more subtle. Lower values of M_{lim} correspond to larger parachutes; larger parachutes dissipate more energy in drag. Higher values of M_{lim} correspond to smaller parachutes, but larger values of wave drag are associated with transonic flow. There is an optimal M_{lim} value of approximately 0.75 for a large range of gross weight values.

Figure 17 shows the variation in H_f at fixed gross weight, as a function of M_{lim} for two different initial altitudes (H_i). This figure shows a classic case of diminishing returns. An increment of 10,000 ft in H_i yields, in the best case, an increment of 3000 ft in H_f. This effect is also attributable to dissipation of energy in drag. For a given true airspeed, as altitude increases and atmospheric density decreases, dynamic pressure and hence lift decrease. The maximum attainable load factor decreases and the radius of curvature of the flightpath increases. An aircraft dropped from higher altitude turns toward the horizontal axis more slowly, and accelerates more quickly. A larger parachute is required to limit Mach number buildup, and the larger parachute dissipates more energy in drag.

Figure 17 also shows that at lower M_{lim} values, a positive increment to H_i actually yields a negative increment to H_f. This effect is not immediately explainable and may be attributable to piloting technique.

Rocket-Assisted Launches

To achieve a H_f of 100,000 ft, the simulation was used to develop techniques for boosting the Apex aircraft with a small rocket motor. The simulation allowed unlimited variations in rocket motor configuration; rocket thrust, attachment point on the Apex aircraft, and attachment angle on the Apex aircraft were infinitely variable. For this study the rocket motor was modeled with its thrust vector passing through the c.g. of the Apex aircraft to simplify the controllability of the Apex aircraft while under rocket boost. The scope of the investigation was limited to two fundamentally different rocket boost techniques.

The first and more conventional boost technique (axial boost) used a relatively low-thrust (435-lb thrust) rocket motor attached to the Apex aircraft to produce thrust along the longitudinal axis of the aircraft. The parachute-assisted launch technique shown in figure 12 was used for the initial part of the launch. The pilot ignited the rocket motor only after he had released the parachute and the Apex aircraft was in its zoom climb. The rocket motor behaved as a high-thrust aircraft engine to boost the Apex aircraft to a higher altitude. The pilot controlled the flightpath angle to keep the Mach number below M_{lim}, and shut down the rocket motor upon reaching the desired altitude. The attainable altitude was limited only by the duration of the rocket burn, or the mass of the rocket motor.

The second rocket-assist technique (normal-axis boost) used a relatively high-thrust (869-lb thrust) rocket motor attached to the Apex aircraft to produce thrust along the normal axis of the aircraft. The pilot released the aircraft from the balloon and ignited the rocket motor when the Apex aircraft had accelerated to $M = 0.25$. The rocket motor behaved as a high-lift augmentation device to directly rotate the velocity vector of the Apex aircraft toward the horizontal axis. The pilot shut down the rocket motor when the flightpath angle reached the horizontal axis. The rotation of the velocity vector to the horizontal axis was executed so quickly that the Apex aircraft did not accelerate to high speed; no parachute was required to keep the Mach number below M_{lim}.

Comparison of Launch Techniques

Figure 18 compares trajectories of the four prototype launch techniques investigated in the simulation study: the unassisted launch, the parachute-assisted launch, the parachute-assisted launch with axial boost, and the normal-axis boost technique. For this comparison, the rocket motor burn time for the axial boost case was experimentally determined to yield the same final altitude as the normal-axis boost case. Both rocket-boost techniques provided simple and efficient means of increasing final altitude, H_f. The normal-axis boost technique required a rocket burn

time of approximately 21 sec and consumed approximately 94 lb of rocket fuel to reach H_f = 102,500 ft; the axial boost technique required a rocket burn time of approximately 32 sec and consumed approximately 70 lb of fuel to reach the same H_f.

Each prototype launch technique shown in figure 18 has its merits and detractions. The unassisted launch technique is, operationally, the simplest technique; there are no special hardware system requirements on the aircraft. However, the distinct disadvantage of this technique is that the Apex aircraft reaches an excessive Mach number that causes loss of performance, potential aerodynamic or structural instability, and possible catastrophic structural failure.

The parachute-assisted launch technique is, operationally, slightly more complex than the unassisted technique; one additional hardware system is required for installation on the aircraft. The parachute-assisted technique solves the overspeed problem in a simple and direct approach. It is also a very flexible technique. Parachute size can be tailored to accommodate a large range of vehicle gross-weight values and maintain the maximum Mach number below any reasonable required value. This technique yielded a higher final altitude than the unassisted launch technique.

The parachute-assisted launch with axial boost is, operationally, the most complex of the launch techniques. This technique requires installation of two hardware systems on the aircraft: a parachute system and a rocket system. The altitude performance of this technique exceeds that of the parachute-assisted technique; final altitudes in excess of 100,000 ft are attainable with small amounts of rocket assist.

The normal-axis boost technique is the most elegant technique and is, operationally, slightly more complex than the unassisted technique. The single required hardware system, a solid-fuel rocket system, is mechanically simple; there are no moving mechanical parts. The normal-axis boost technique attains the final altitude condition most directly and quickly. As with the axial-boost technique, final altitudes in excess of 100,000 ft are attainable with small amounts of rocket assist.

CONCLUDING REMARKS

A real-time piloted simulation at the NASA Dryden Flight Research Facility was used to demonstrate the feasibility of deploying an Apex research aircraft at high altitude with a high-altitude balloon. The simulation model for the Apex aircraft was based on modifications to an existing commercially produced sailplane. Aerodynamic modifications to the basic sailplane included applying supercritical airfoil gloves over the existing wing and tail surfaces. The aerodynamic model of the modified aircraft was developed using a combination of computational techniques, wind-tunnel test results, flight test results of the basic sailplane, and handbook methods. The aerodynamic model included significant Mach number and Reynolds number effects at high altitude.

The balloon-assisted deployment technique developed in this simulation study merits consideration as a deployment technique for atmospheric science mission and other high-altitude aircraft. The benign maneuvering loads and limited Mach numbers encountered in the parachute-assisted, axial boost, and normal-axis boost launch techniques place no special requirements on onboard scientific measurement hardware. The balloon-assisted deployment technique is potentially useful for deploying an unpowered aircraft very quickly and cost-effectively, or for deploying a powered aircraft to altitude with its full fuel capacity held in reserve. The balloon-assisted deployment technique also has the potential to be the first stage of a multistage extreme-altitude powered aircraft system.

Deploying an aerodynamic research aircraft such as the Apex aircraft with a high-altitude balloon has great potential for acquiring low Reynolds number, transonic aerodynamic research data very quickly and cost-effectively. These research data can be used to validate and calibrate wind-tunnel and computational techniques used in the development of high-altitude aircraft.

Dryden Flight Research Facility
National Aeronautics and Space Administration
Edwards, California, December 5, 1991

REFERENCES

Carmichael, B. H., *Low Reynolds Number Airfoil Survey Volume I*, NASA CR-165803, 1981.

Chambers, Alan, and R. Dale Reed, "A Very High Altitude Aircraft for Global Climate Research," *Unmanned Systems*, vol. 8, no. 3, Summer 1990, pp. 14–19.

DeLaurier, J., B. Gagnon, J. Wong, R. Williams, and C. Hayball, "Research on the Technology of an Airplane Concept for a Stationary High-Altitude Relay Platform (SHARP)," *Canadian Aeronautics and Space Journal*, vol. 32, no. 1, Mar. 1986, pp. 26–46.

Drela, Mark, and Michael B. Giles, "Viscous-Inviscid Analysis of Transonic and Low Reynolds Number Airfoils," *AIAA Journal*, vol. 25, no. 10, Oct. 1987, pp. 1347–1355.

Ember, Lois R., Patricia L. Layman, Wil Lepkowski, and Pamela S. Zurer, "Tending the Global Commons," *Chemical & Engineering News*, vol. 64, no. 47, Nov. 24, 1986, pp. 14–64.

Global Stratospheric Change: Requirements for a Very-High-Altitude Aircraft for Atmospheric Research, NASA CP-10041, 1989.

Henderson, Breck W., "Boeing Condor Raises UAV Performance Levels," *Aviation Week & Space Technology*, vol. 132, no. 16, Apr. 23, 1990, pp. 36–38.

Jones, Robert T., and Doris Cohen, *High Speed Wing Theory*, Princeton Aeronautical Paperbacks, Princeton University Press, Princeton, NJ, 1960.

Kennelly, Robert A., Ilan M. Kroo, James M. Strong, and Ralph L. Carmichael, *Transonic Wind Tunnel Test of a 14% Thick Oblique Wing*, NASA TM-102230, 1990.

LinAir for the Macintosh, Version 3.3 – LinAir Pro., Desktop Aeronautics, Stanford, CA, 1987.

Maine, Richard E., and Kenneth W. Iliff, *Application of Parameter Estimation to Aircraft Stability and Control*, NASA RP-1168, 1986.

Mueller, Thomas J., *Low Reynolds Number Vehicles*, AGARDograph No. 288, AGARD-AG-288, 1985.

PANDA – A Program for Analysis and Design of Airfoils, Version 1.6., Desktop Aeronautics, Stanford, CA, 1988.

Peterson, Laurence E., "Window on the Cosmos," *Aerospace America*, vol. 29, no. 11, Nov. 1991, pp. 40–44.

Reed, R. Dale, "High-Flying Mini-Sniffer RPV: Mars Bound?," *Astronautics and Aeronautics*, vol. 16, no. 6, June 1978, pp. 26–39.

Roskam, Jan, *Airplane Flight Dynamics and Automatic Flight Controls*, Roskam Aviation and Engineering Corp., Ottawa, KS, 1979.

Russell, P., J. Langford, J. Anderson, D. Lux, D.W. Hall, and S. Wegener, "Advanced Aircraft for Atmospheric Research," AIAA-91-3162, Sept. 1991.

Sim, Alex G., *Flight Characteristics of a Modified SGS 1-36 Sailplane at Low and Very High Angles of Attack*, NASA TP-3022, 1990.

Sim, Alex G., *Modeling, Simulation, and Flight Characteristics of an Aircraft Designed to Fly at 100,000 Feet*, NASA TM-104236, 1991.

U. S. Standard Atmosphere, 1962, U.S. Government Printing Office, Washington, DC.

Table 1. Physical and mass properties of the Apex and Schweizer SGS 1-36 aircraft.

	Apex aircraft	Schweizer SGS 1-36 sailplane
S, ft^2	163.94	140.72
b, ft	46.17	46.17
$\bar{c}$, ft	3.55	3.28
mg, lb	869.00	710.00
I_{XX}, slug-ft^2	1261.00	1006.00
I_{XZ}, slug-ft^2	67.20	32.00
I_{YY}, slug-ft^2	771.00	494.00
I_{ZZ}, slug-ft^2	2003.00	1494.00

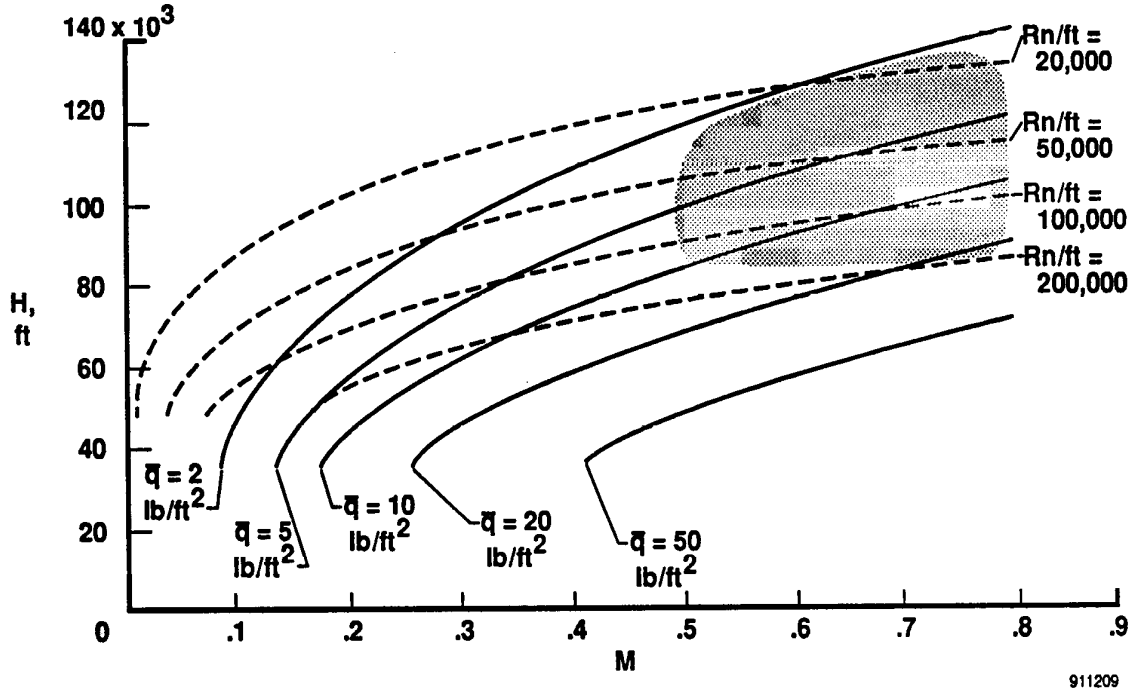

Figure 1. Generalized flight envelope for high-altitude aircraft.

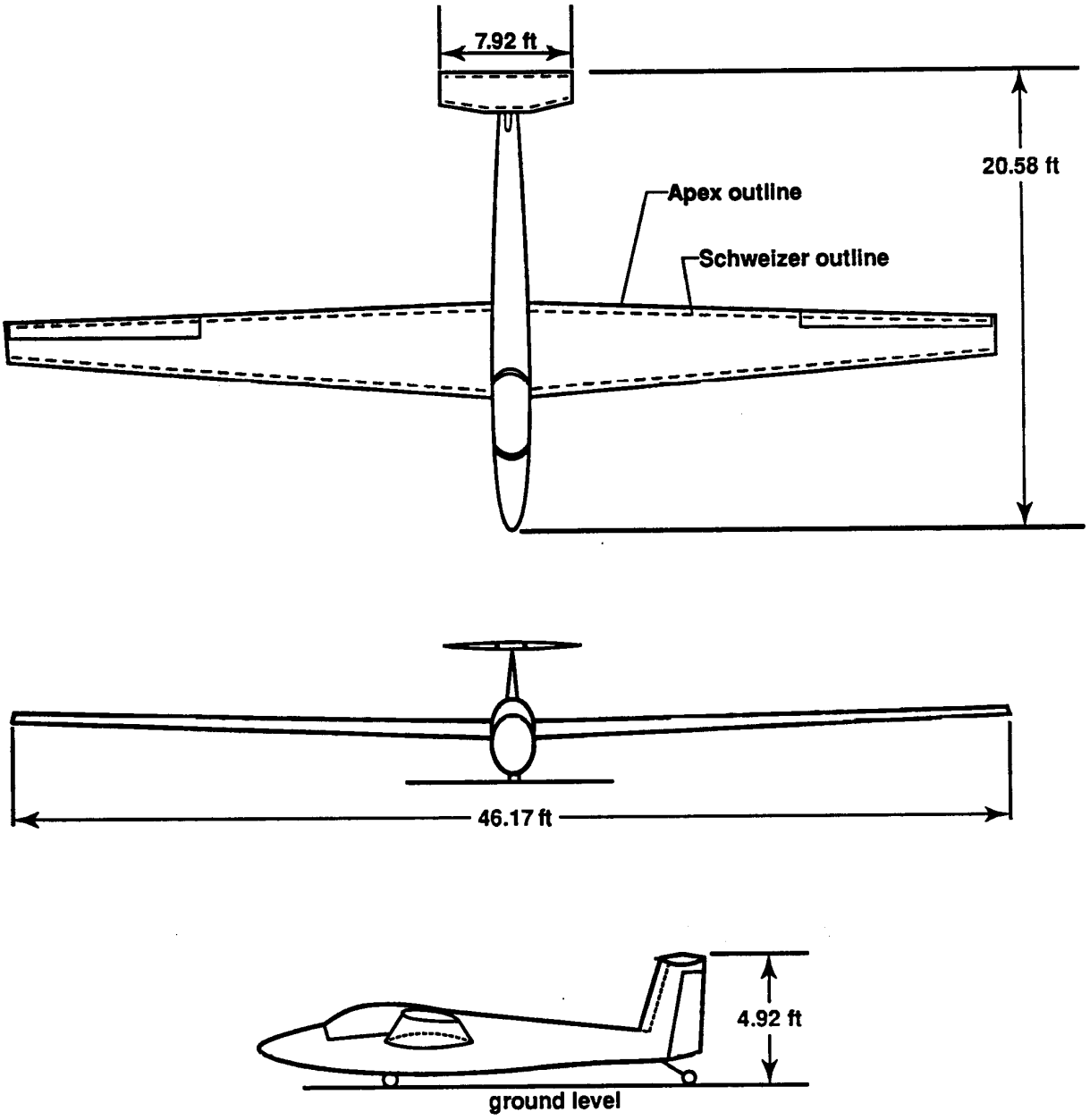

Figure 2. Apex and Schweizer SGS 1-36 aircraft geometry.

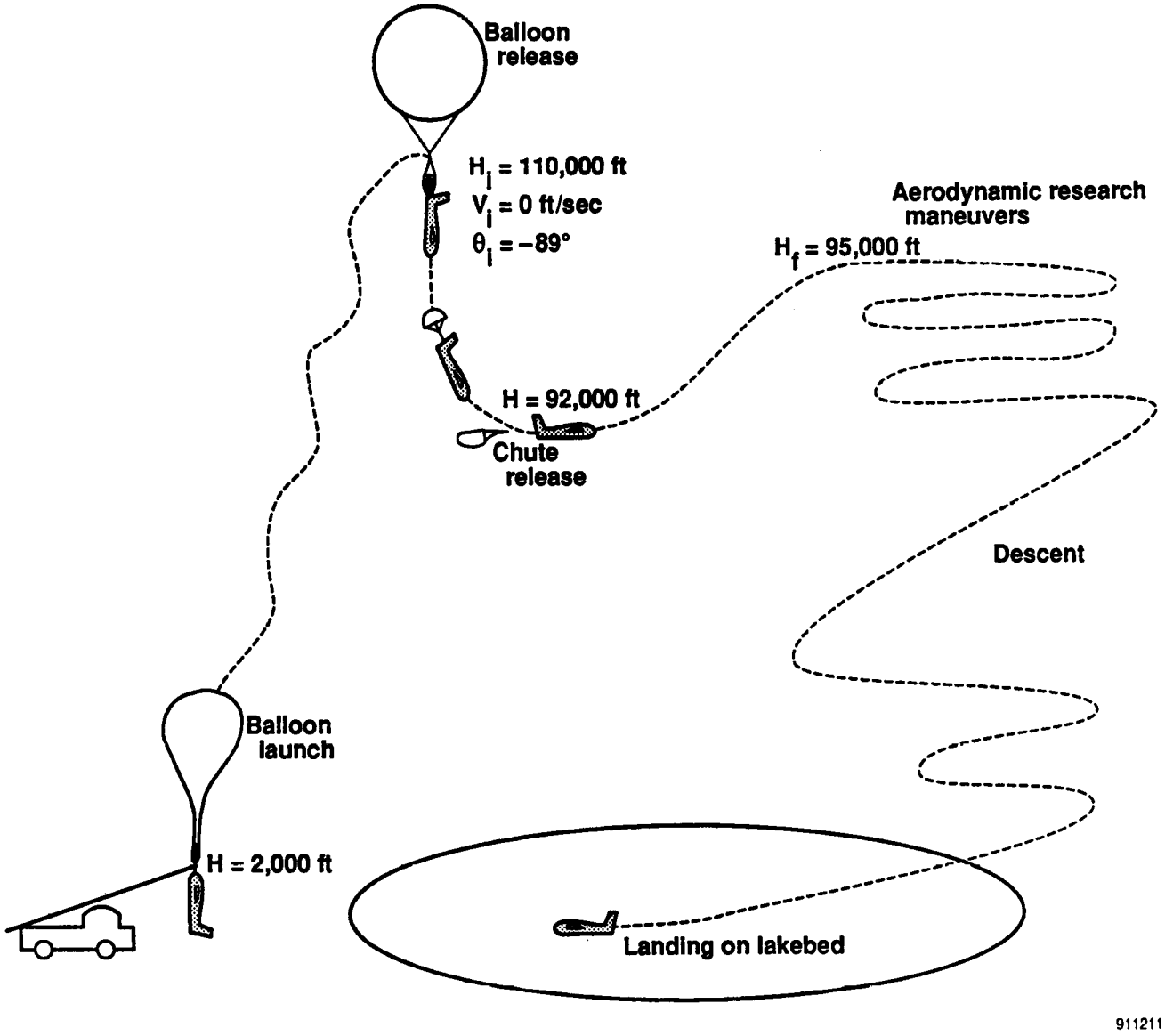

Figure 3. Schematic outline of a proposed Apex research flight.

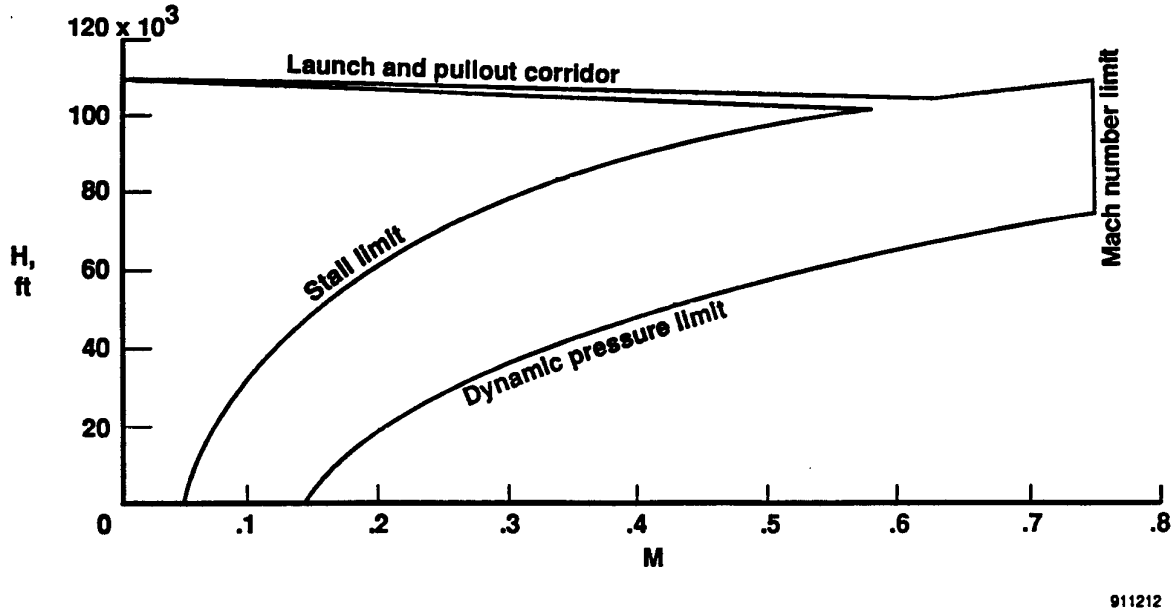

Figure 4. Apex flight envelope.

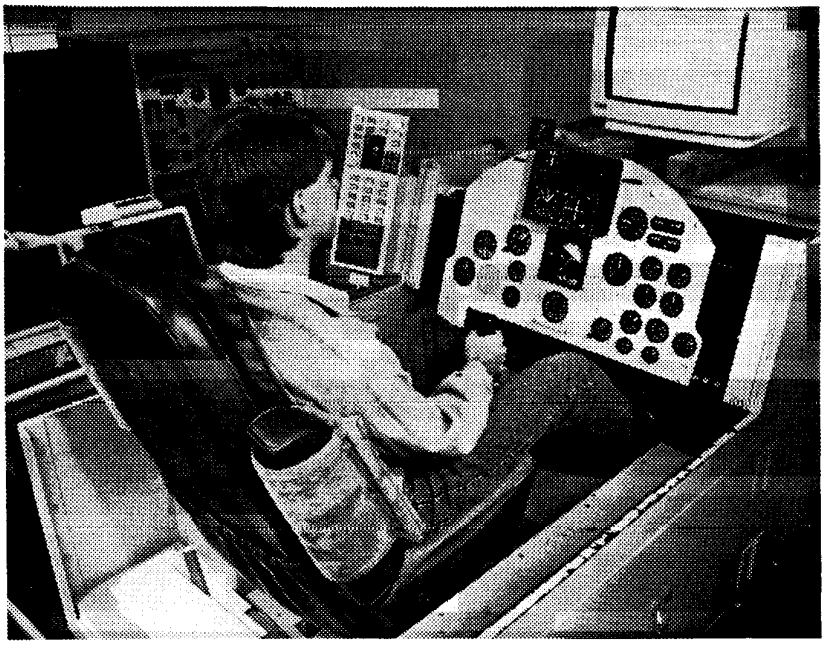

EC 91 660–1

Figure 5. Apex simulator cockpit.

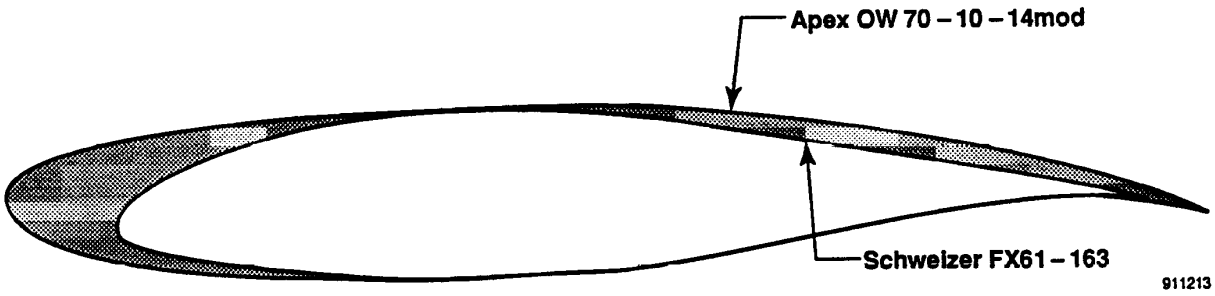

Figure 6. Comparison of Schweizer FX61-163 and Apex OW 70-10-14mod airfoil geometries.

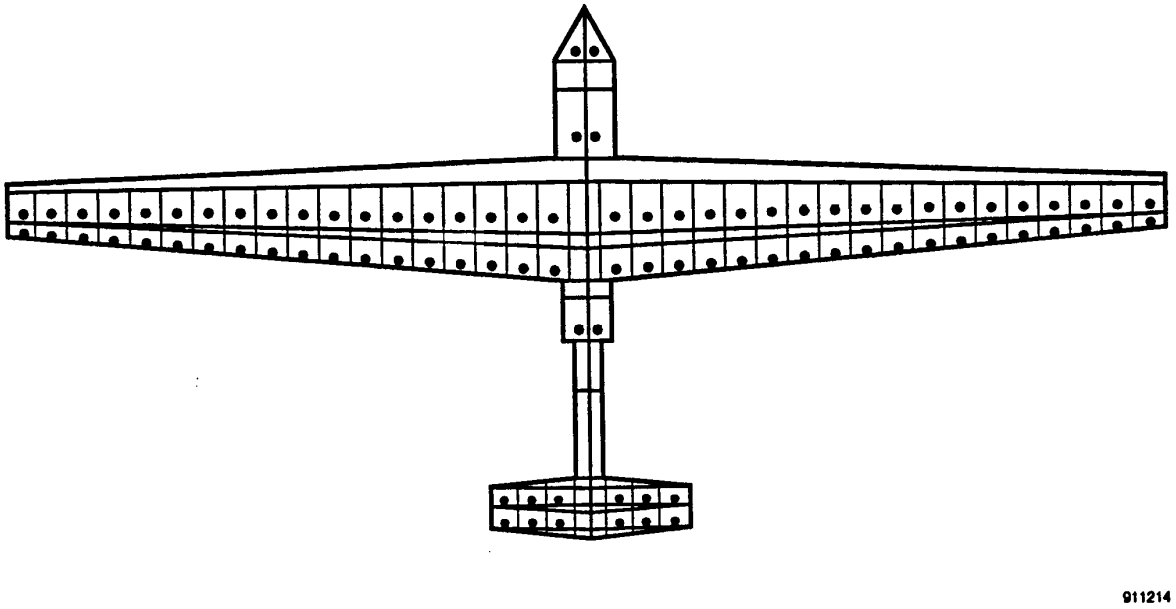

Figure 7. LinAir paneled model of Apex aircraft.

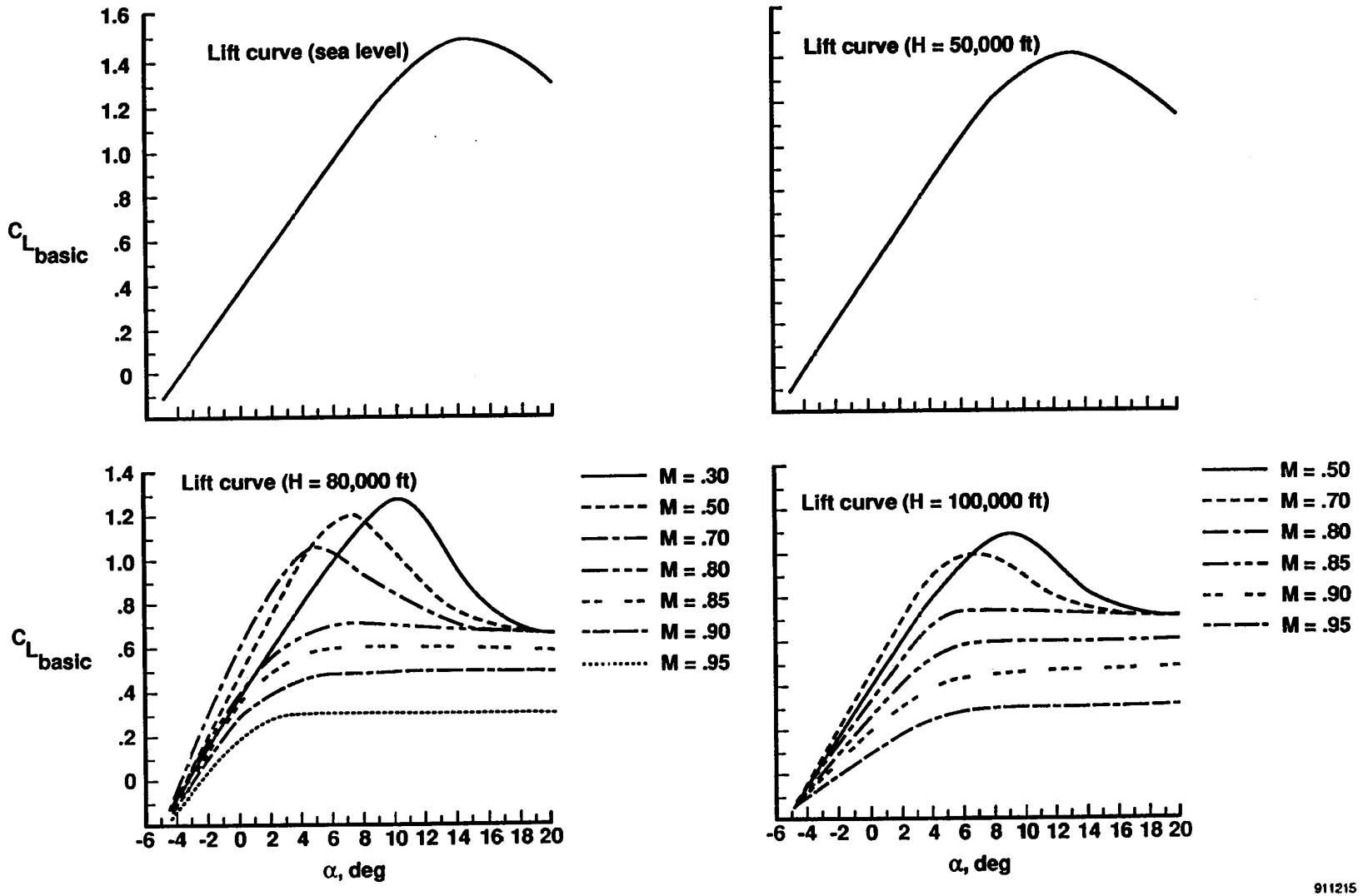

Figure 8. Apex lift coefficient model.

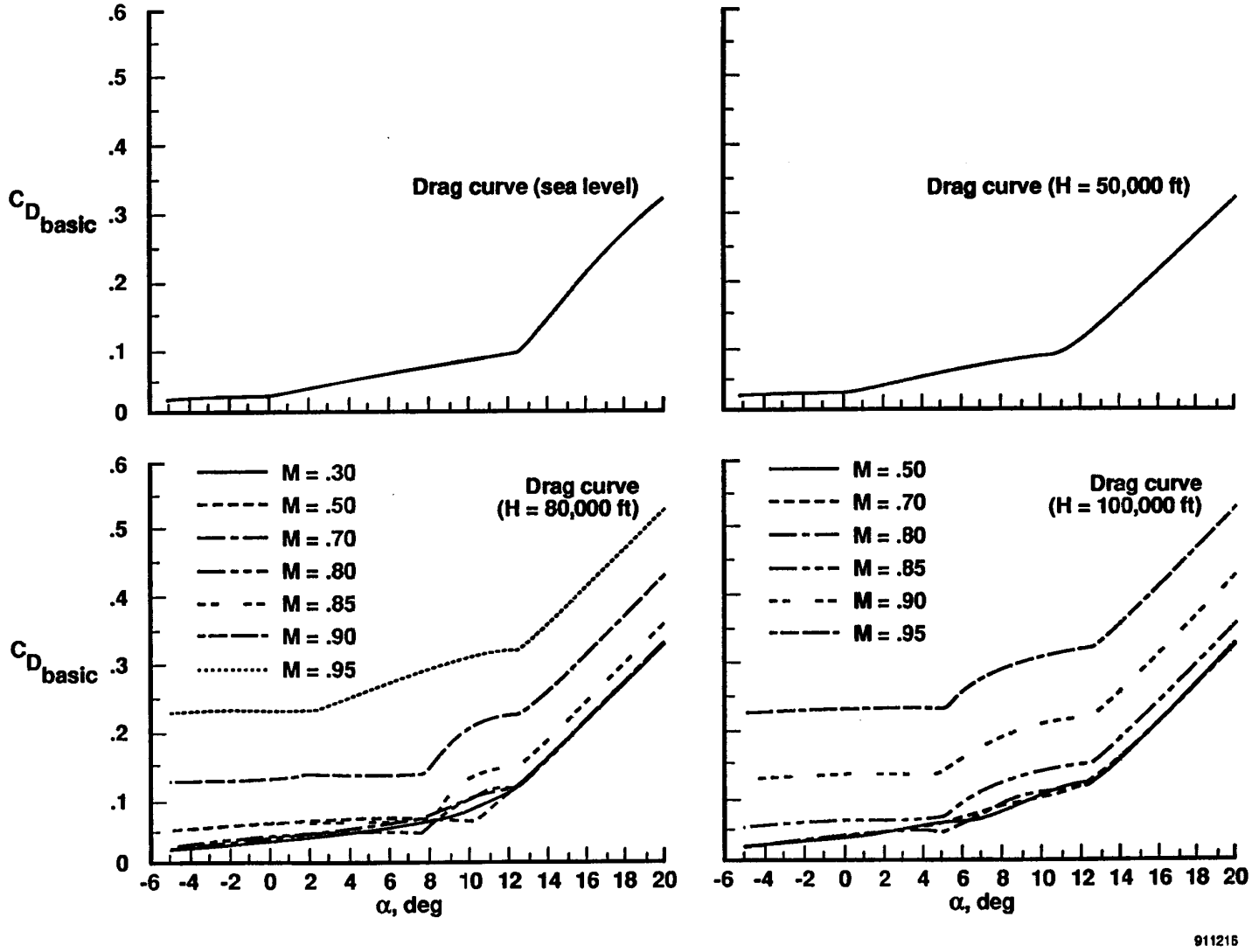

Figure 9. Apex drag coefficient model.

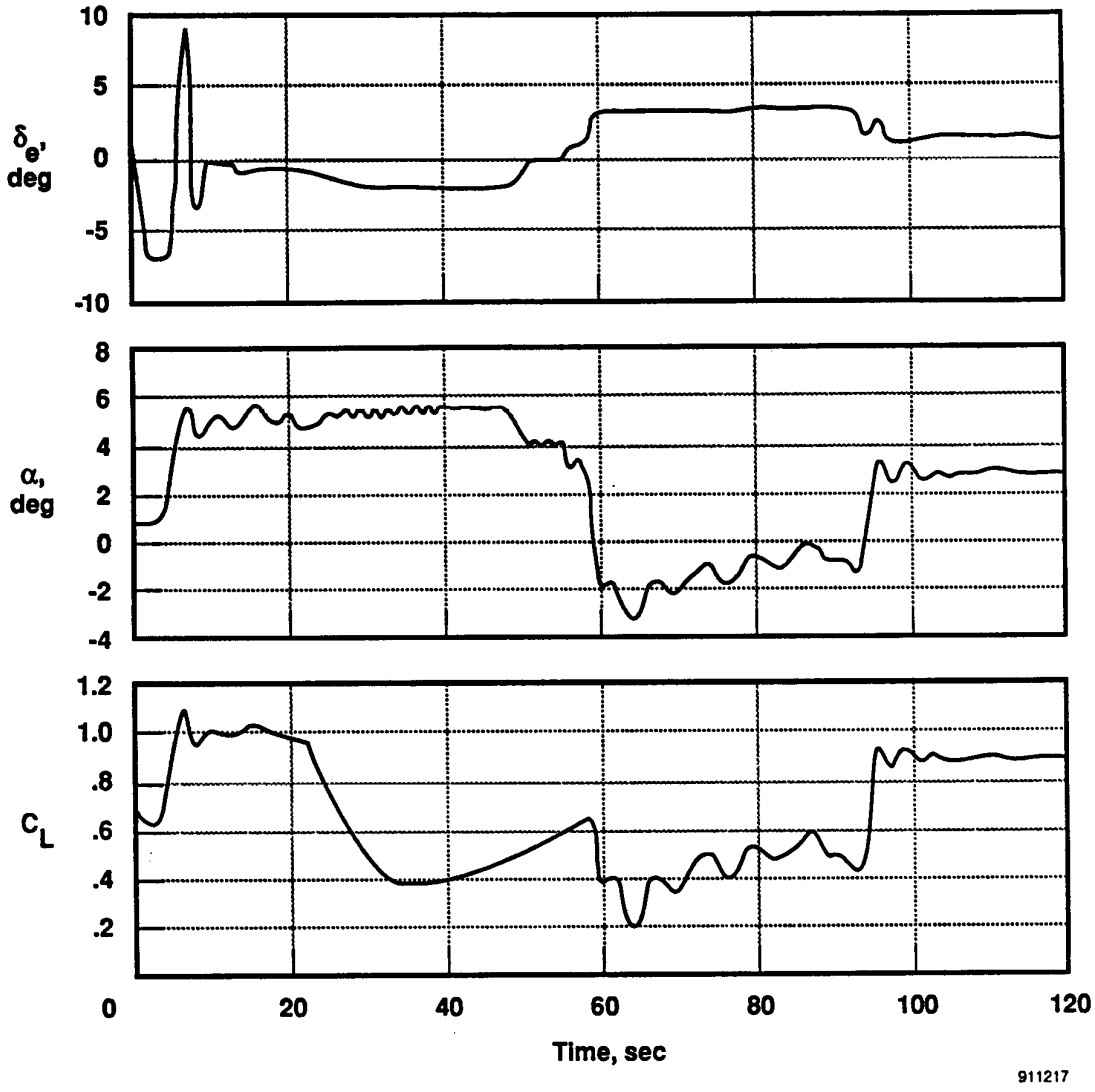

(a)

Figure 10. Simulation time history of unassisted balloon launch from 110,000 ft.

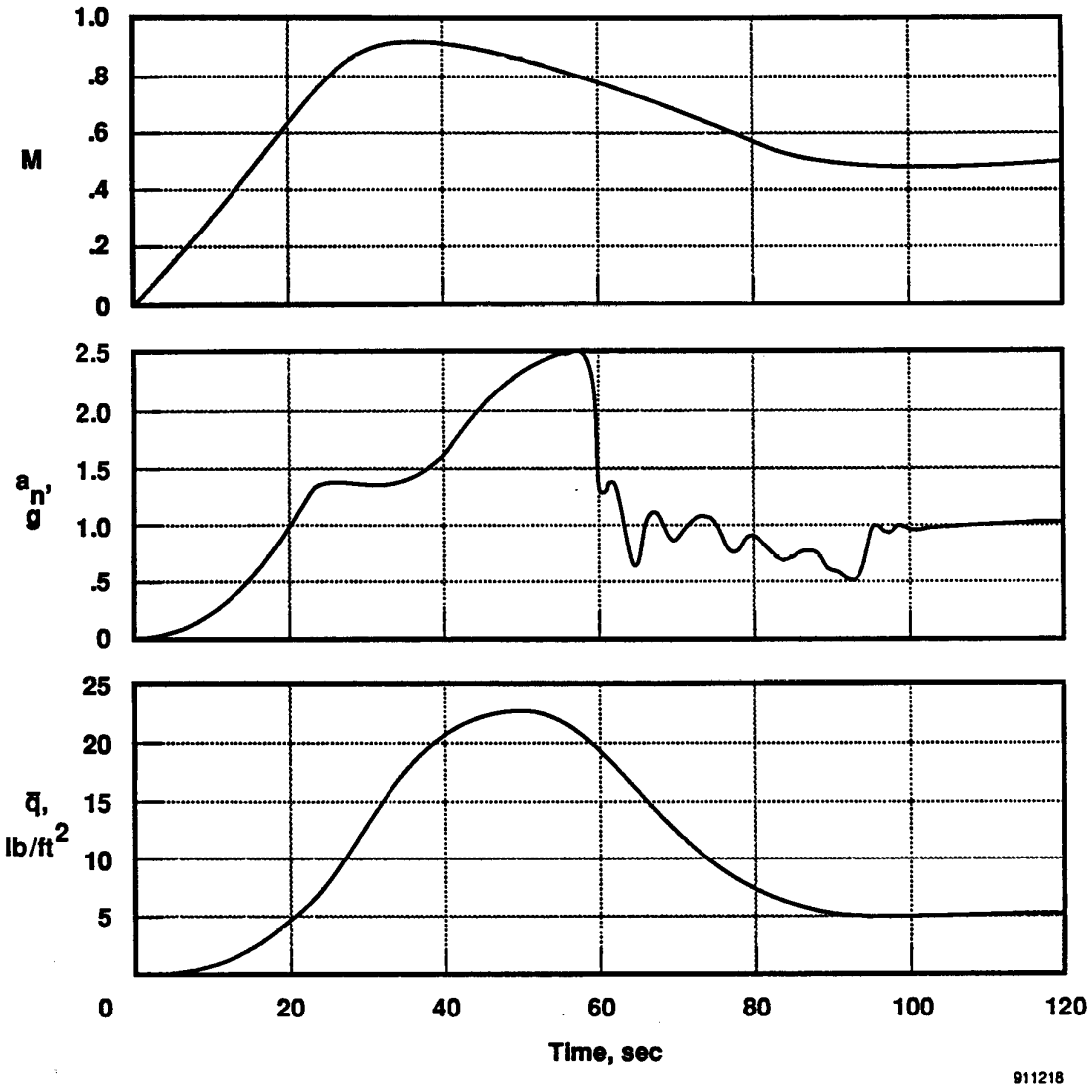

(b)

Figure 10. Continued.

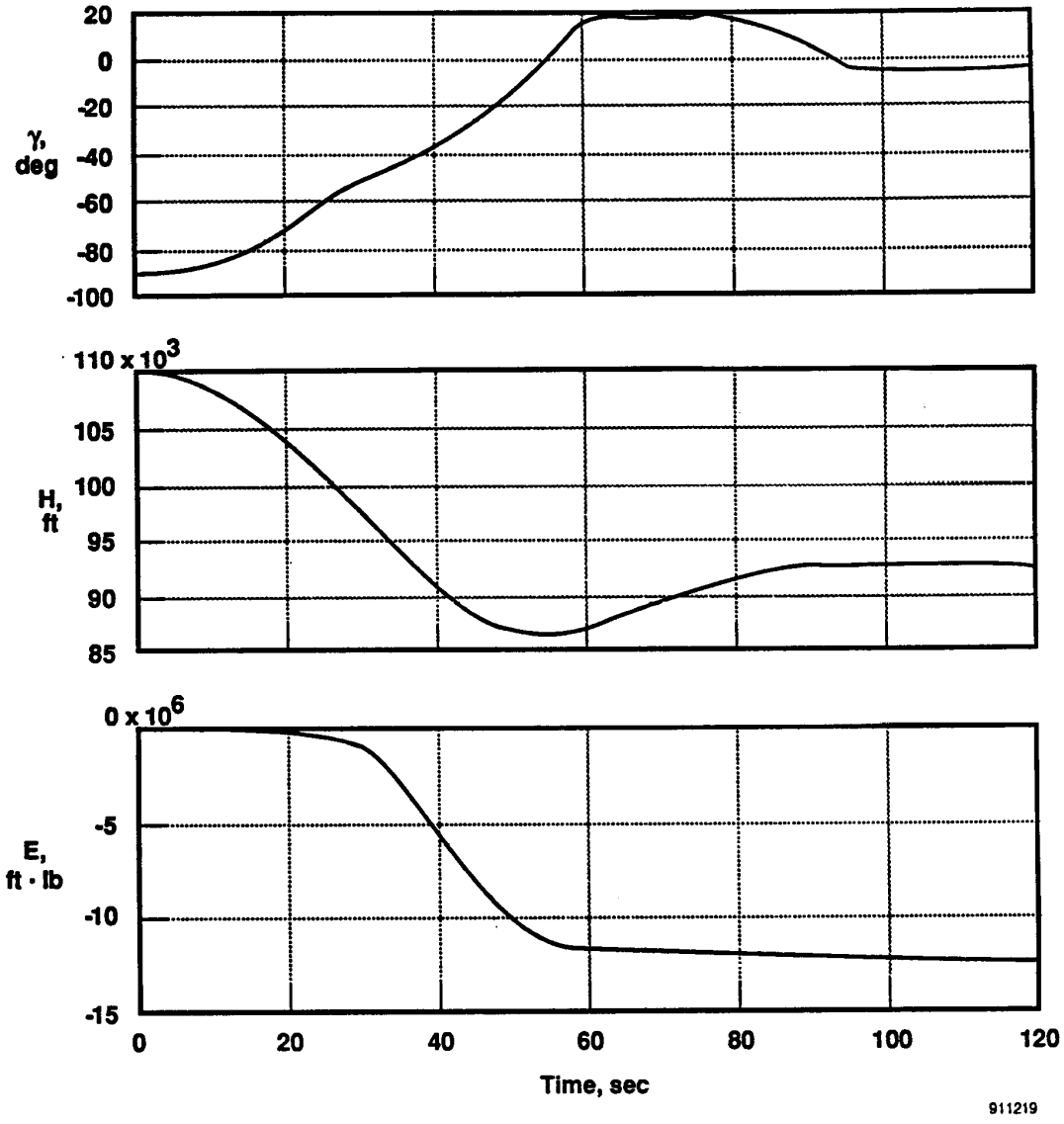

(c)

Figure 10. Concluded.

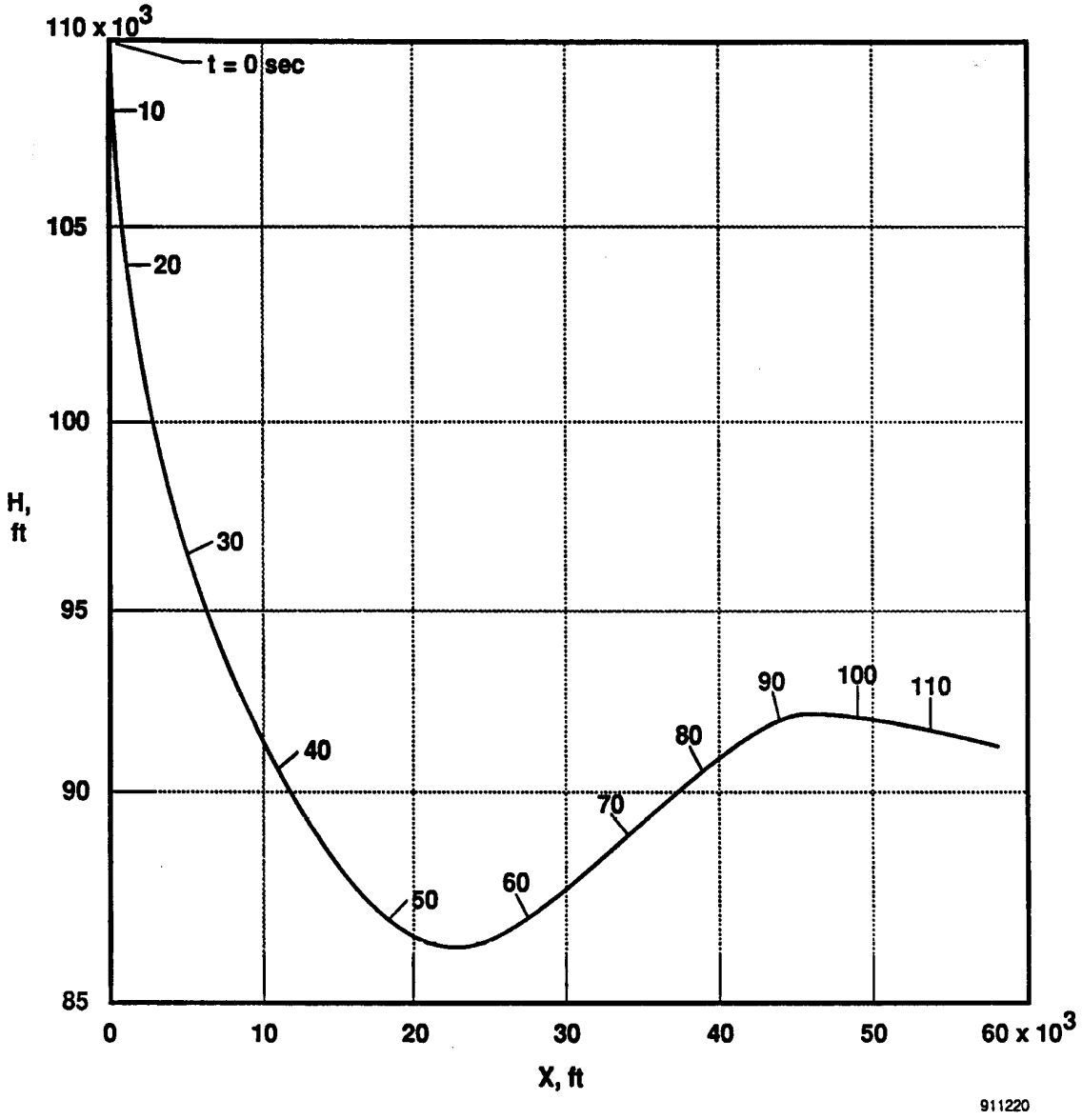

Figure 11. Simulation trajectory of unassisted balloon launch from 110,000 ft.

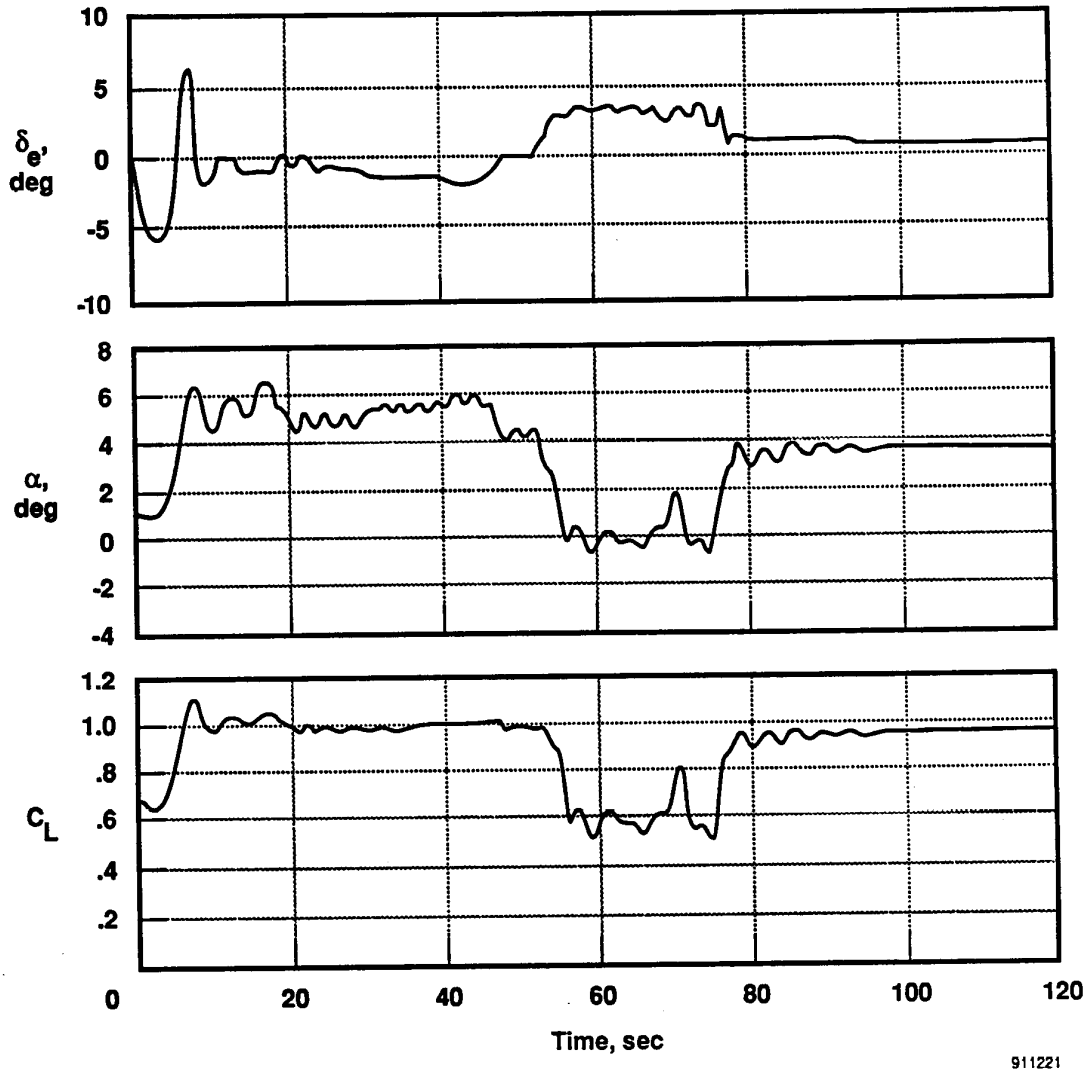

(a)

Figure 12. Simulation time history of parachute-assisted balloon launch from 110,000 ft.

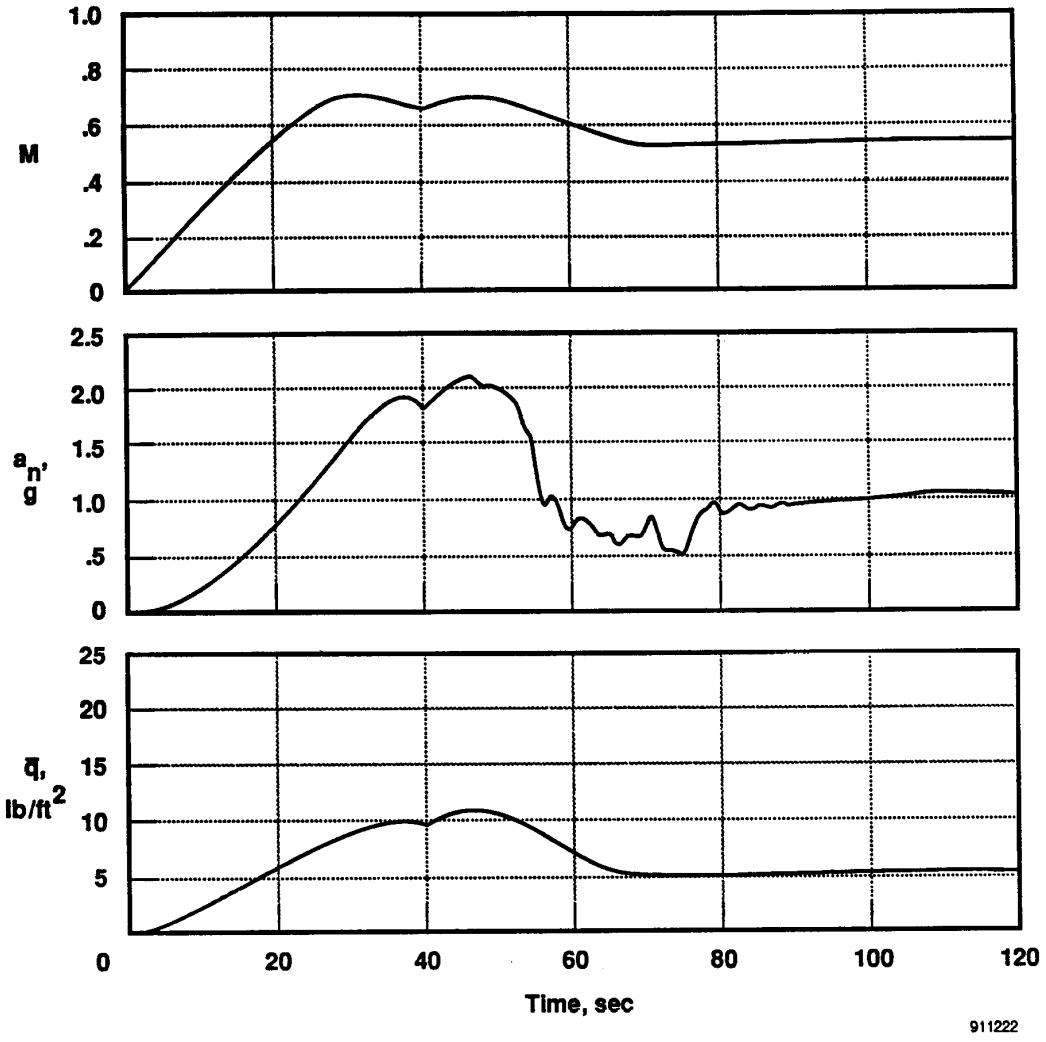

(b)

Figure 12. Continued.

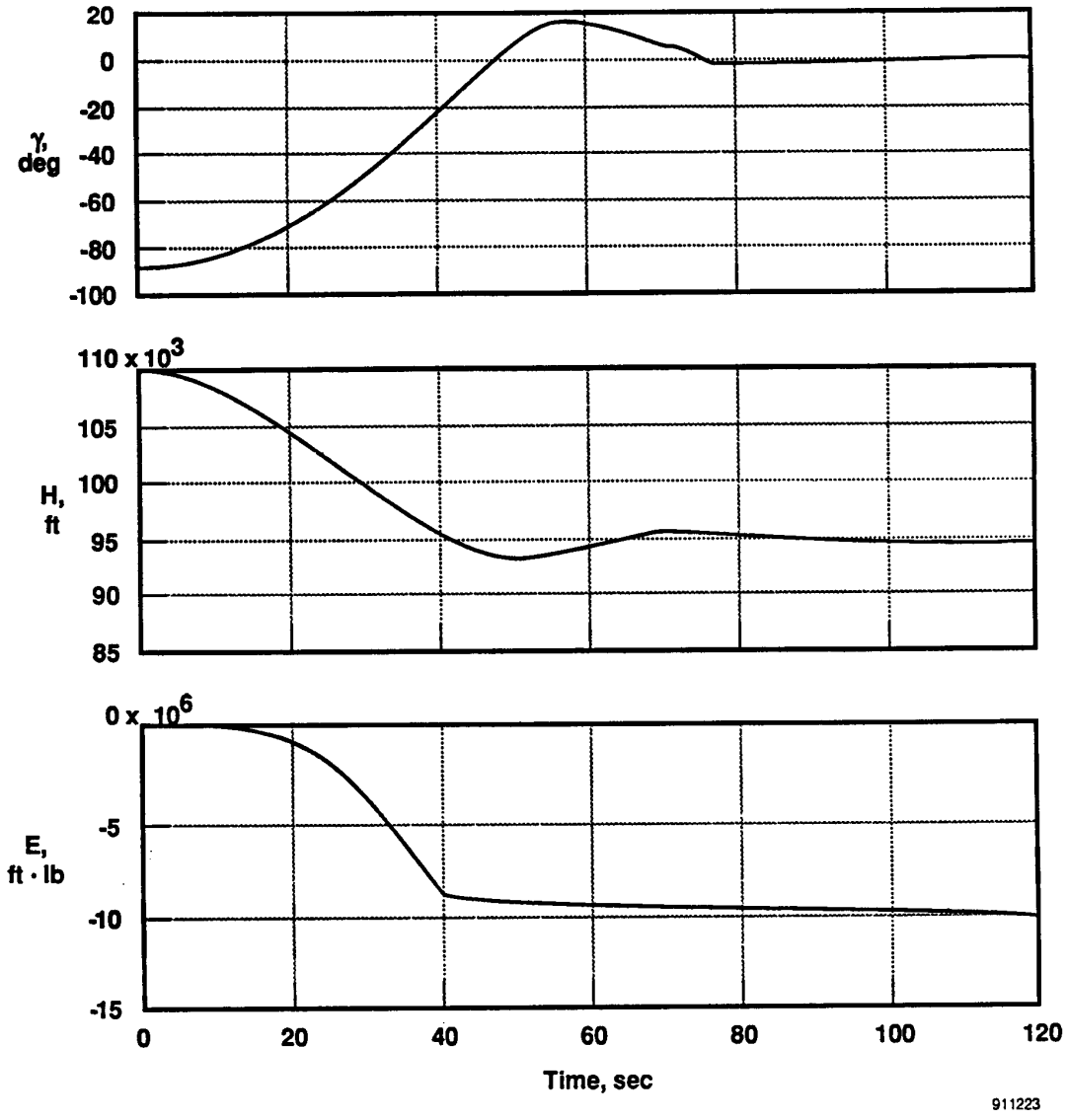

(c)

Figure 12. Concluded.

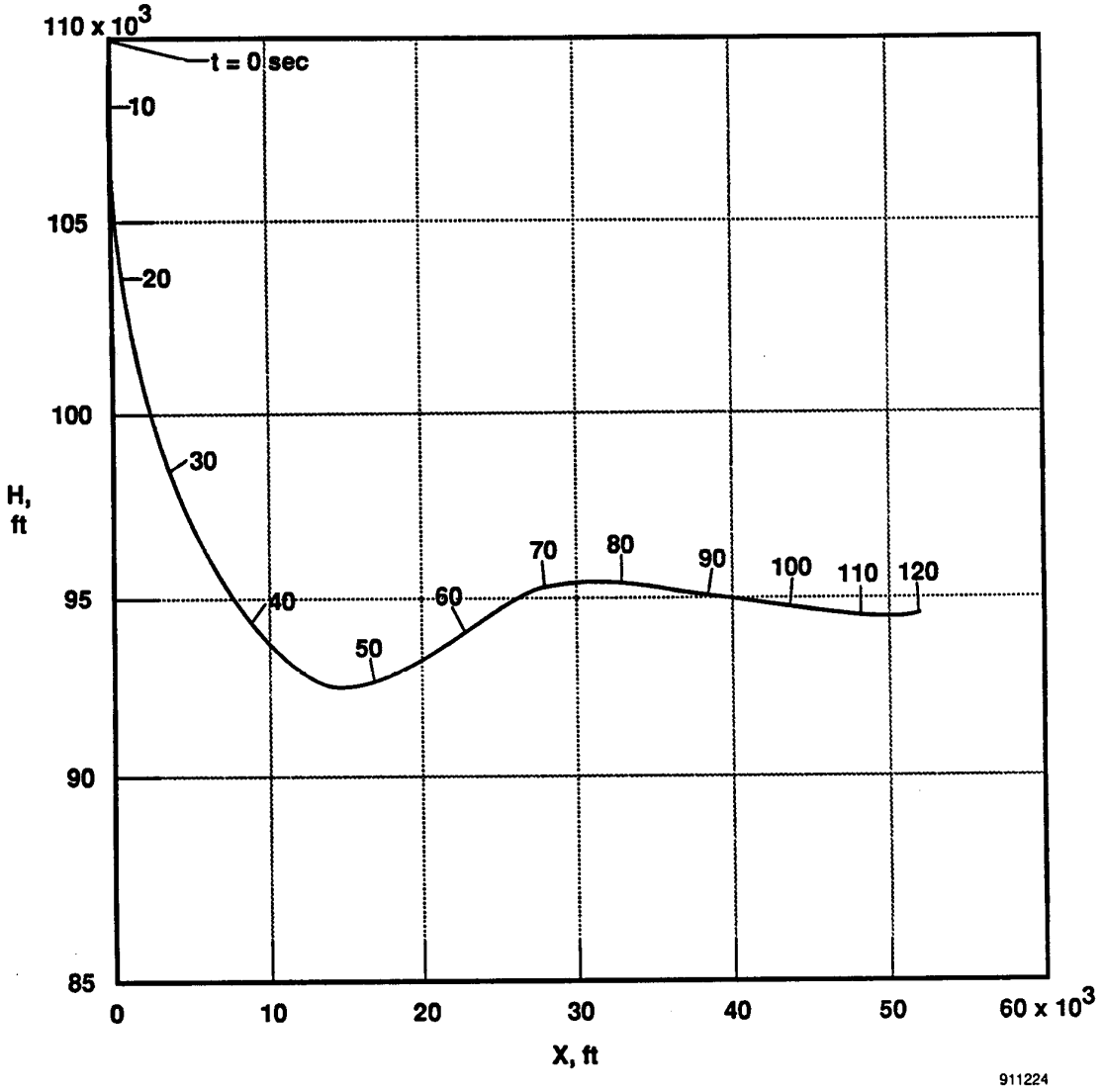

Figure 13. Simulation trajectory of parachute-assisted balloon launch from 110,000 ft.

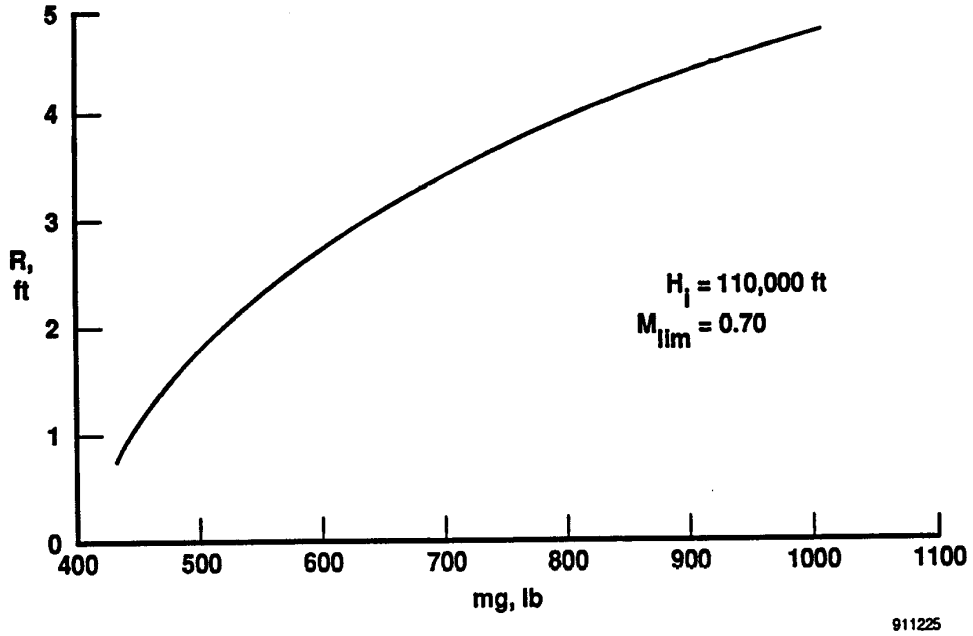

Figure 14. Parachute radius required as a function of aircraft gross weight for H_i = 110,000 ft, M_{lim} = 070.

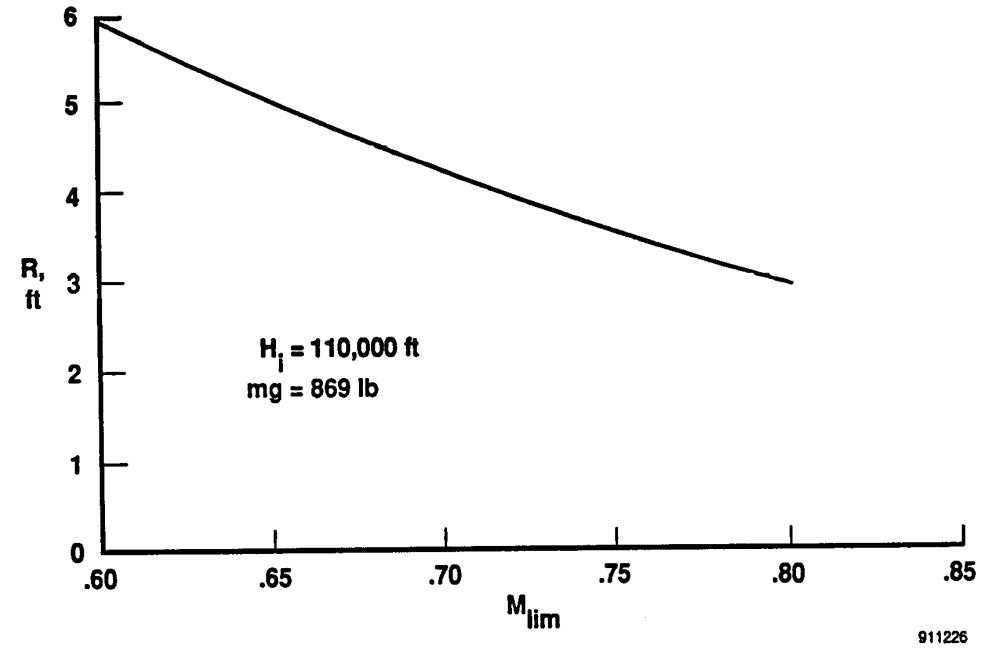

Figure 15. Parachute radius required as a function of limit Mach number for H_i = 110,000 ft, mg = 869 lb.

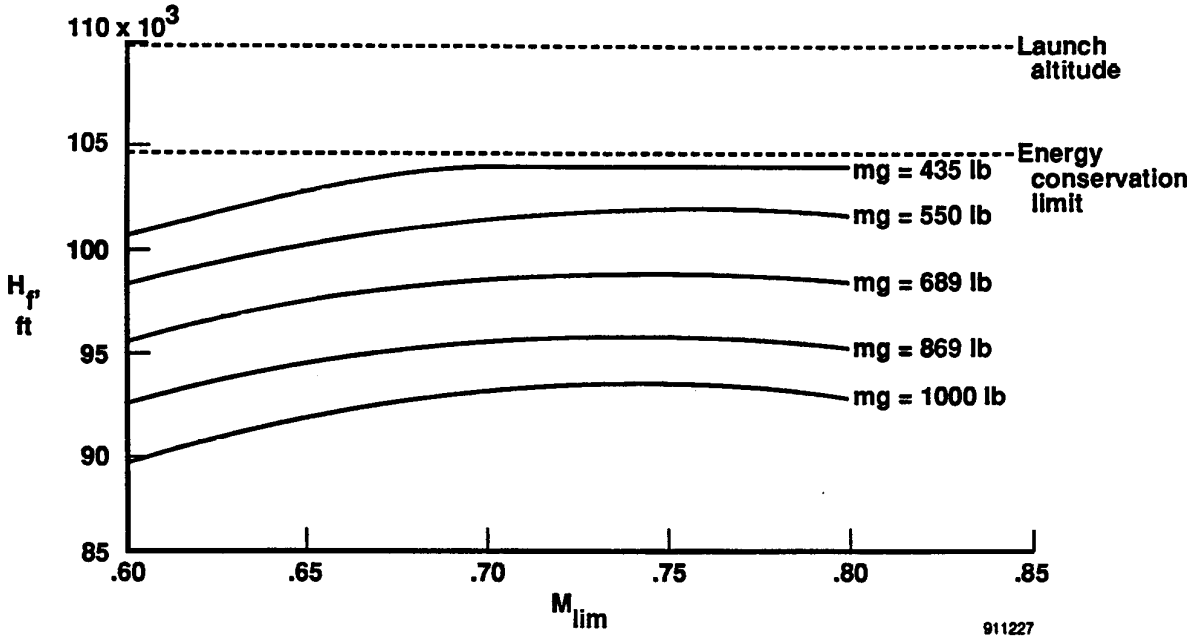

Figure 16. Final altitude as a function of limit Mach number for several gross weights.

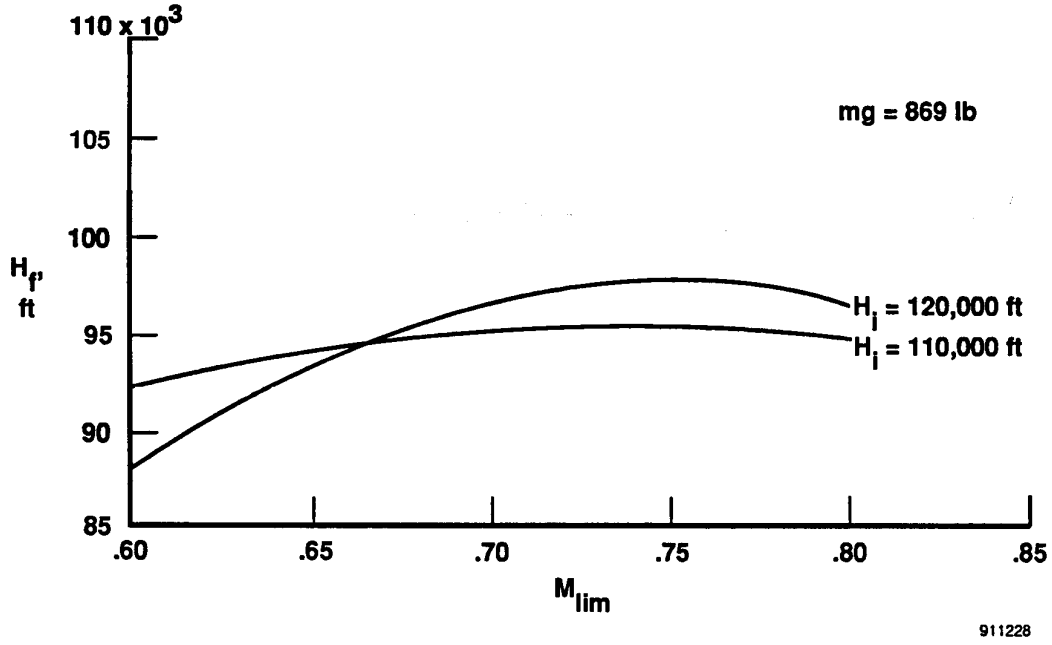

Figure 17. Final altitude as a function of limit Mach number for two initial altitudes.

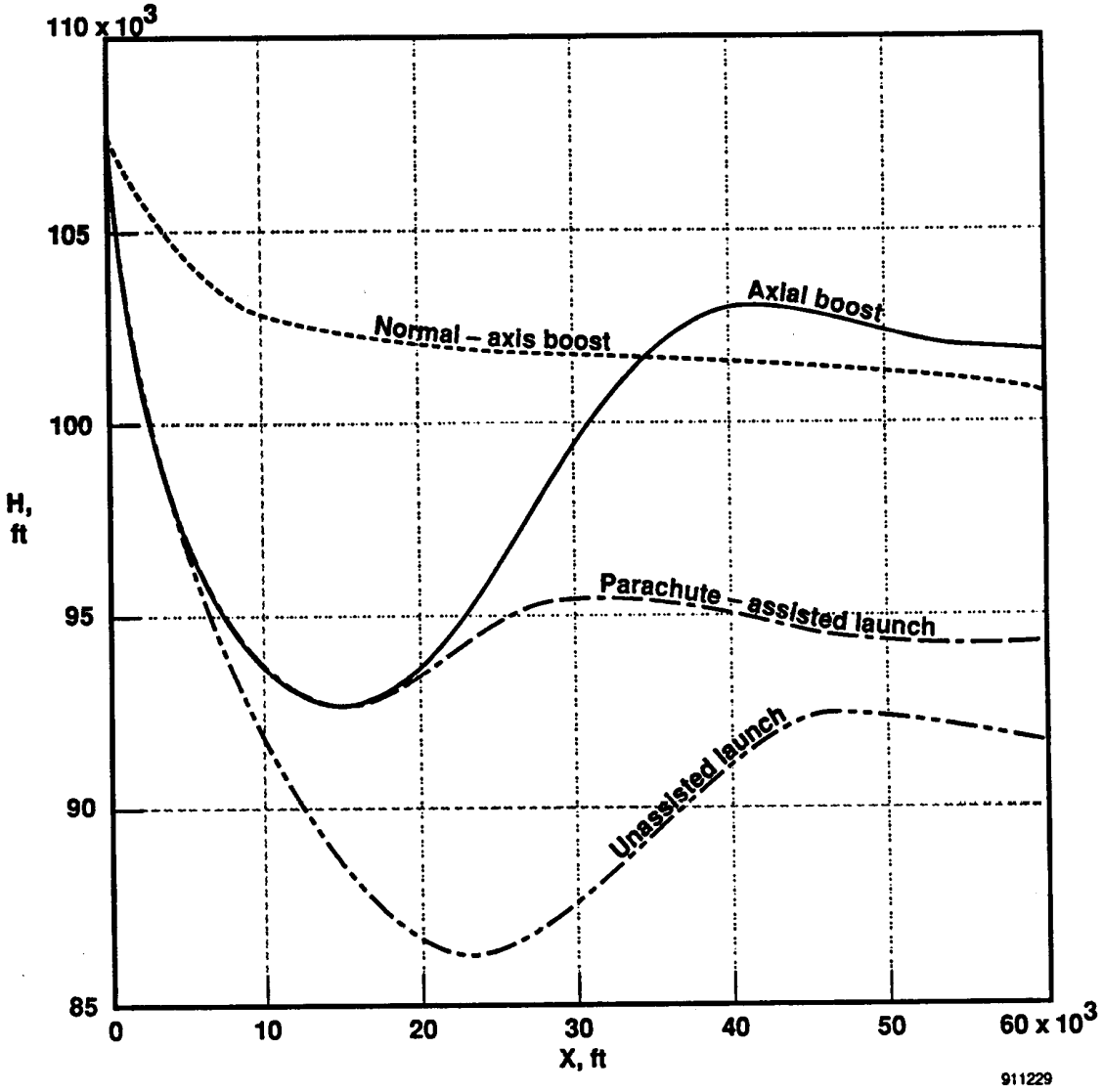

Figure 18. Comparison of trajectories for four different launch techniques.

REPORT DOCUMENTATION PAGE

Form Approved
OMB No. 0704-0188

1. AGENCY USE ONLY *(Leave blank)*	2. REPORT DATE	3. REPORT TYPE AND DATES COVERED
	January 1992	Technical Memorandum

4. TITLE AND SUBTITLE

Piloted Simulation Study of a Balloon-Assisted Deployment of an Aircraft at High Altitude

5. FUNDING NUMBERS

WU-505-68-50

6. AUTHOR(S)

James Murray, Timothy Moes, Ken Norlin, Jeffrey Bauer (Dryden Flight Research Facility, Edwards, California)
Robert Geenen, Bryan Moulton (PRC Inc., Edwards, California)
Stephen Hoang (Dryden Flight Research Facility, Edwards, California)

7. PERFORMING ORGANIZATION NAME(S) AND ADDRESS(ES)

NASA Dryden Flight Research Facility
P.O. Box 273
Edwards, California 93523-0273

8. PERFORMING ORGANIZATION REPORT NUMBER

H-1785

9. SPONSORING/MONITORING AGENCY NAME(S) AND ADDRESS(ES)

National Aeronautics and Space Administration
Washington, DC 20546-0001

10. SPONSORING/MONITORING AGENCY REPORT NUMBER

NASA TM-104245

11. SUPPLEMENTARY NOTES

Prepared for presentation at the Sixth Workshop on Civilian and Military Needs for Automated Instrument Platforms in the 1990s and Beyond, Association for Unmanned Vehicle Systems, Silicon Valley Chapter, January 28–30, 1992, Menlo Park, California.

12a. DISTRIBUTION/AVAILABILITY STATEMENT

Unclassified — Unlimited
Subject Category 05

12b. DISTRIBUTION CODE

13. ABSTRACT ***(Maximum 200 words)***

A piloted simulation at the NASA Dryden Flight Research Facility (NASA Dryden) was used to study the feasibility of a balloon-assisted deployment of a research aircraft at high altitude. In the simulation study, an unmanned, modified sailplane was carried to 110,000 ft with a high-altitude balloon and released in a nose-down attitude. A remote pilot controlled the aircraft through a pullout and then executed a zoom climb to a trimmed, 1-g flight condition. A small parachute was used to limit the Mach number during the pullout to avoid adverse transonic effects. The use of a small rocket motor was investigated for increasing the maximum attainable altitude.

Aerodynamic modifications to the basic sailplane included applying supercritical airfoil gloves over the existing wing and tail surfaces. The aerodynamic model of the simulated aircraft was based on low Reynolds number wind-tunnel tests and computational techniques, and included significant Mach number and Reynolds number effects at high altitude.

Parametric variations were performed to study the effects of launch altitude, gross weight, Mach number limit, and parachute size on the maximum attainable stabilized altitude. A test altitude of approximately 95,000 ft was attained, and altitudes in excess of 100,000 ft were attained with small amounts of rocket motor assist.

14. SUBJECT TERMS

Atmospheric science; High-altitude aircraft; Low Reynolds number aerodynamics; Remotely piloted vehicle; Simulation

15. NUMBER OF PAGES

33

16. PRICE CODE

A03

17. SECURITY CLASSIFICATION OF REPORT	18. SECURITY CLASSIFICATION OF THIS PAGE	19. SECURITY CLASSIFICATION OF ABSTRACT	20. LIMITATION OF ABSTRACT
Unclassified	Unclassified	Unclassified	Unlimited